Geomagnetic field intensity changes in the Central Mediterranean between 1500 BCE and 150 CE: implications for the Levantine Iron Age Anomaly evolution.

M. Rivero-Montero[1], M. Gómez-Paccard[1], D. Kondopoulou[2], E. Tema[3,4], F.J. Pavón-Carrasco[1,5], E. Aidona[2], S.A. Campuzano[1], A. Molina-Cardín[1,5], M.L. Osete[1,5], A. Palencia-Ortas[1,5], F. Martín-Hernández[1,5], F. Rubat-Borel[6], M. Venturino[7]

[1]Instituto de Geociencias IGEO (CSIC-UCM), c/Doctor Severo Ochoa, 7, Edificio Entrepabellones 7 y 8, Ciudad Universitaria, 28040 Madrid, Spain.

E-mail addresses: m.rivero@csic.es; mgomezpaccard@csic.es; fjpavon@ucm.es; saioa.arquero@igeo.ucm-csic.es; amcardin@ucm.es; mlosete@ucm.es; ali@ucm.es; fatima@ucm.es.

[2]Aristotle University of Thessaloniki, Department of Geophysics, School of Geology, 54124 Thessaloniki, Greece. E-mail: despi@geo.auth.gr; aidona@geo.auth.gr.

[3]Università degli Studi di Torino, Dipartimento di Scienze della Terra, Via Valperga Caluso 35, 10125 Torino, Italy. E-mail: evdokia.tema@unito.it.

[4]Alpine Laboratory of Paleomagnetism ALP-CIMaN, Via G.U. Massa 6, 12016 Peveragno, Italy

[5]Facultad de CC. Físicas, Dpto. de Física de la Tierra y Astrofísica, Universidad Complutense de Madrid, Avd. Complutense s/n, 28040-Madrid, Spain.

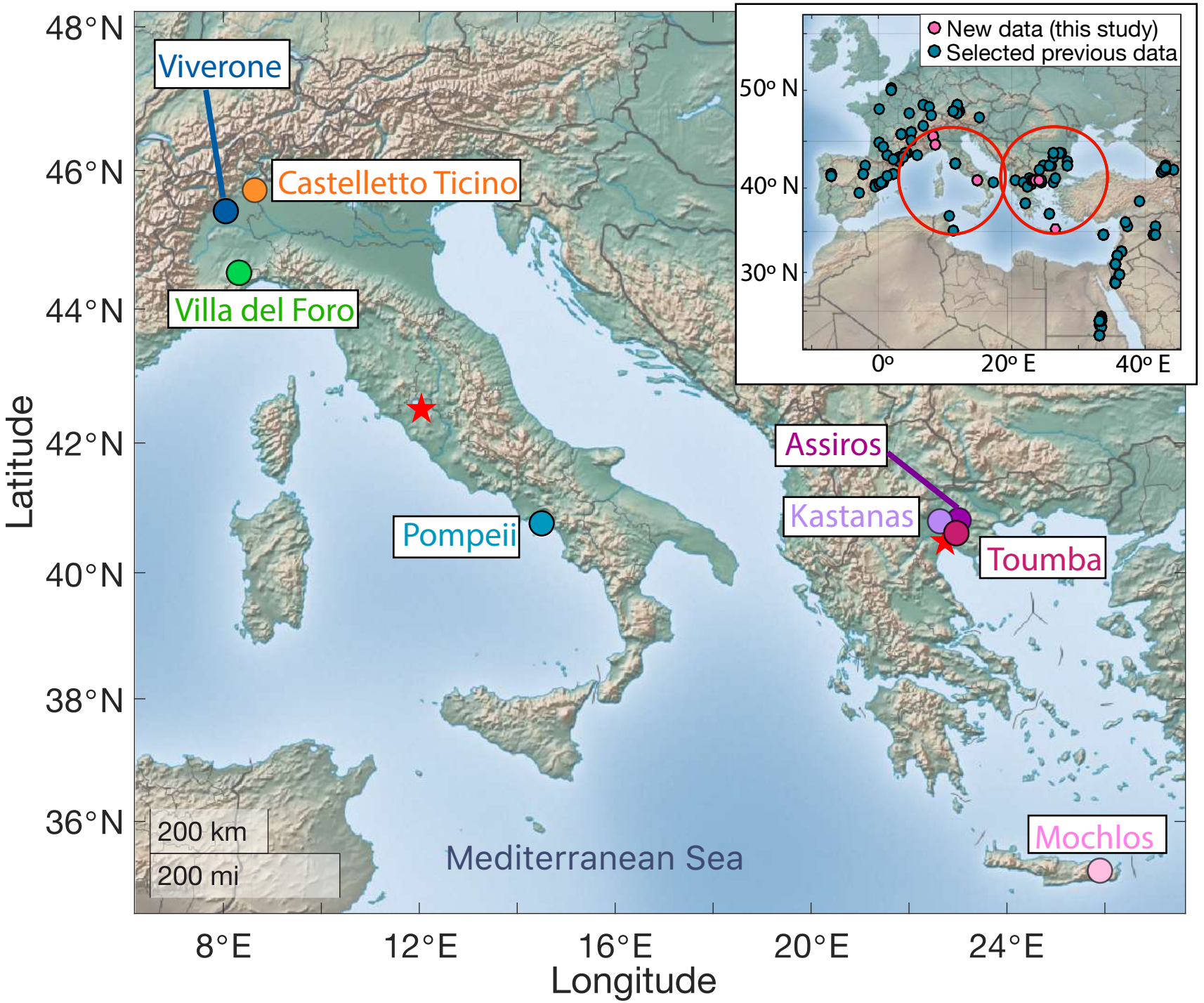
Viverone
Castelletto Ticino
Villa del Foro
Pompeii
Assiros
Kastanas
Toumba
Mochlos
Mediterranean Sea
200 km
200 mi
48°N
46°N
44°N
42°N
40°N
38°N
36°N
Latitude
8°E
12°E
16°E
20°E
24°E
Longitude
New data (this study)
Selected previous data
50° N
40° N
30° N
0°
20° E
40° E


A)
Mochlos
Kastanas
GR-KA
02-B
GR-KA
03-A
Assiros
GR-AS
Ø9
Toumba
1 cm
B)
CT: Briccola
CT: Novella
Villa del Foro
VDF
1 cm
Pompeii
05
Viverone

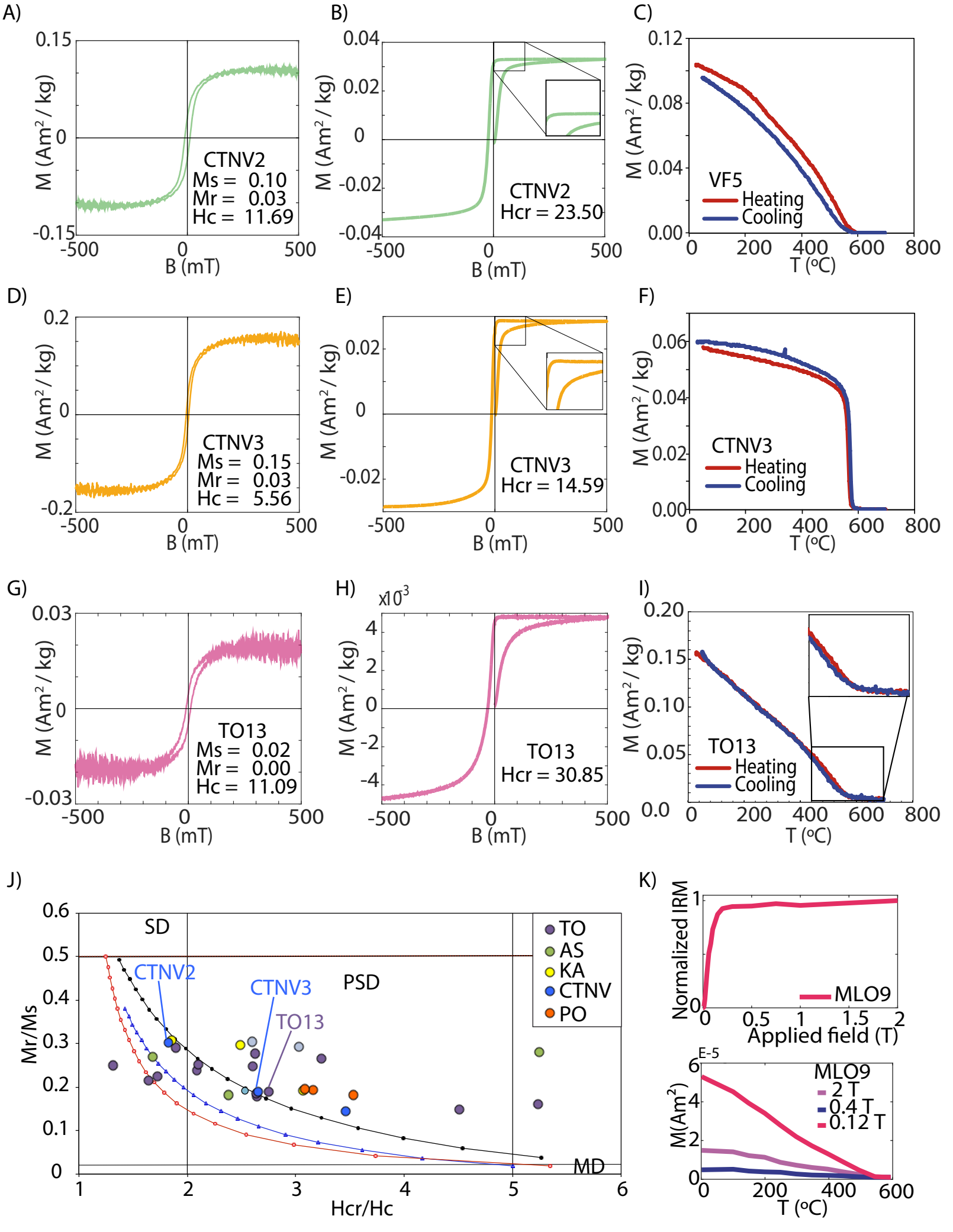
A)
B)
C)
D)
E)
F)
G)
H)
I)
J)
K)
M (Am² / kg)
B (mT)
T (°C)
CTNV2
Ms = 0.10
Mr = 0.03
Hc = 11.69
CTNV2
Hcr = 23.50
VF5
Heating
Cooling
CTNV3
Ms = 0.15
Mr = 0.03
Hc = 5.56
CTNV3
Hcr = 14.59
CTNV3
Heating
Cooling
TO13
Ms = 0.02
Mr = 0.00
Hc = 11.09
x10⁻³
TO13
Hcr = 30.85
TO13
Heating
Cooling
SD
PSD
MD
CTNV2
CTNV3
TO13
TO
AS
KA
CTNV
PO
Mr/Ms
Hcr/Hc
Normalized IRM
MLO9
Applied field (T)
E-5
MLO9
2 T
0.4 T
0.12 T
M(Am²)
T (°C)

A)

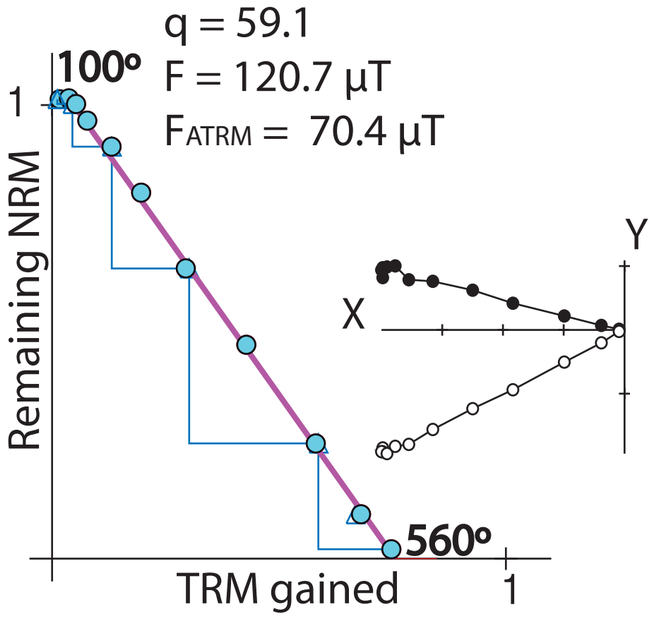
Specimen: TO-10A
NRM = 5.2•10-3 Am2/kg
q = 59.1
F = 120.7 µT
FATRM = 70.4 µT
100º
560º
Remaining NRM
TRM gained
1
X
Y

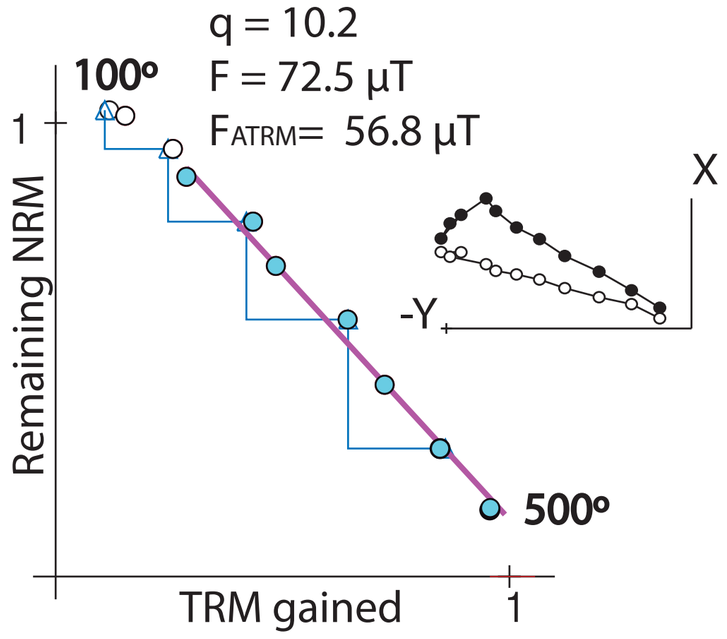
Specimen: MLO-3A
NRM = 1.2•10-4 Am2/kg
q = 10.2
F = 72.5 µT
FATRM= 56.8 µT
100º
500º
Remaining NRM
TRM gained
1
X
-Y

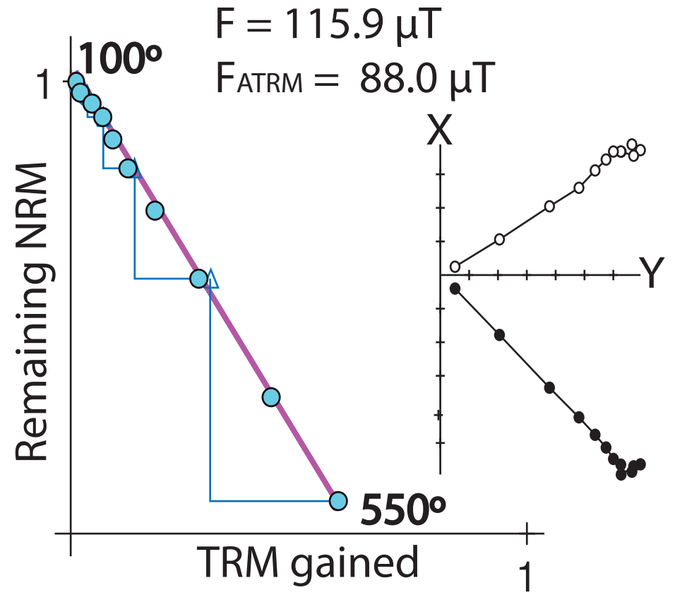
Specimen: AS-9D
NRM = 1.1•10-2 Am2/kg
q = 79.6
F = 115.9 µT
FATRM = 88.0 µT
100º
550º
Remaining NRM
TRM gained
1
X
Y

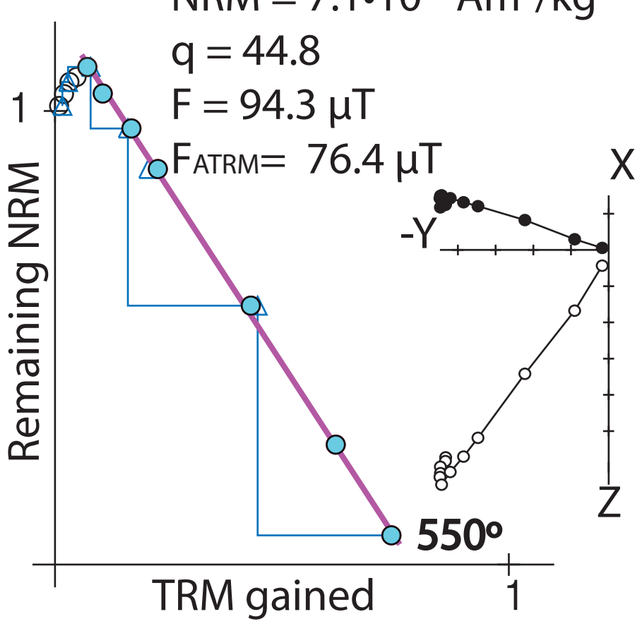
Specimen: AS-4D
NRM = 7.1•10-4 Am2/kg
q = 44.8
F = 94.3 µT
FATRM= 76.4 µT
550º
Remaining NRM
TRM gained
1
X
-Y
Z

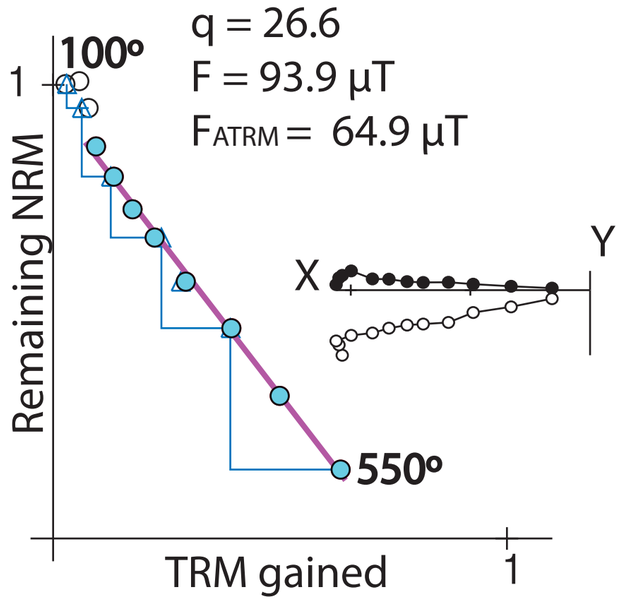
Specimen: KA-7C
NRM = 2.3•10-3 Am2/kg
q = 26.6
F = 93.9 µT
FATRM = 64.9 µT
100º
550º
Remaining NRM
TRM gained
1
X
Y

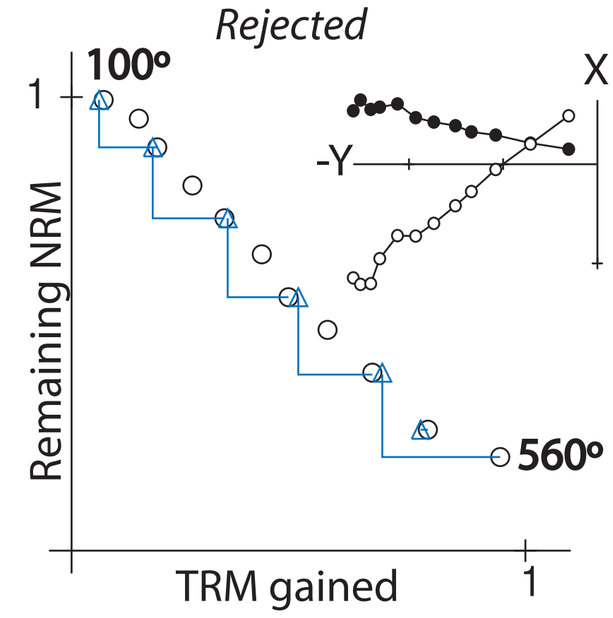
Specimen: TO-12A
NRM = 3.0•10-4 Am2/kg
Rejected
100º
560º
Remaining NRM
TRM gained
1
X
-Y

B)

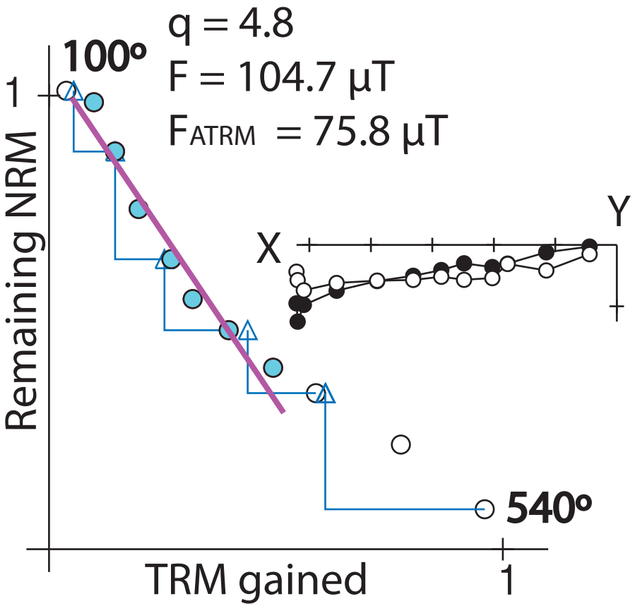
Specimen: CTBR-7A
NRM = 5.8•10-4 Am2/kg
q = 4.8
F = 104.7 µT
FATRM = 75.8 µT
100º
540º
Remaining NRM
TRM gained
1
X
Y

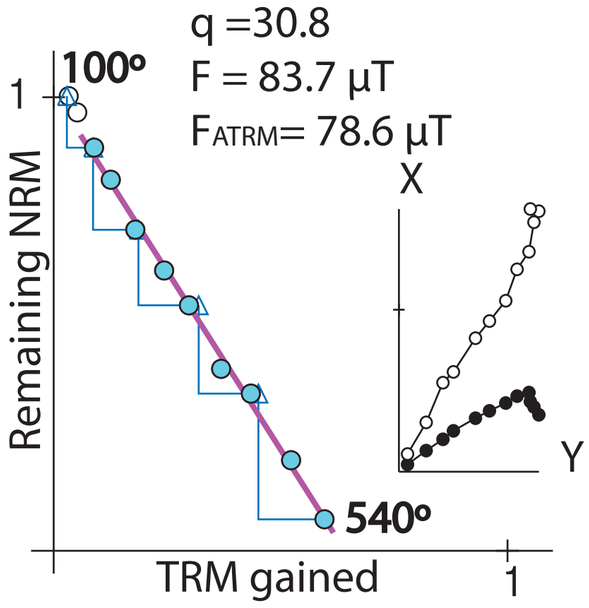
Specimen: CTNV-2A
NRM = 1.0•10-3 Am2/kg
q =30.8
F = 83.7 µT
FATRM= 78.6 µT
100º
540º
Remaining NRM
TRM gained
1
X
Y

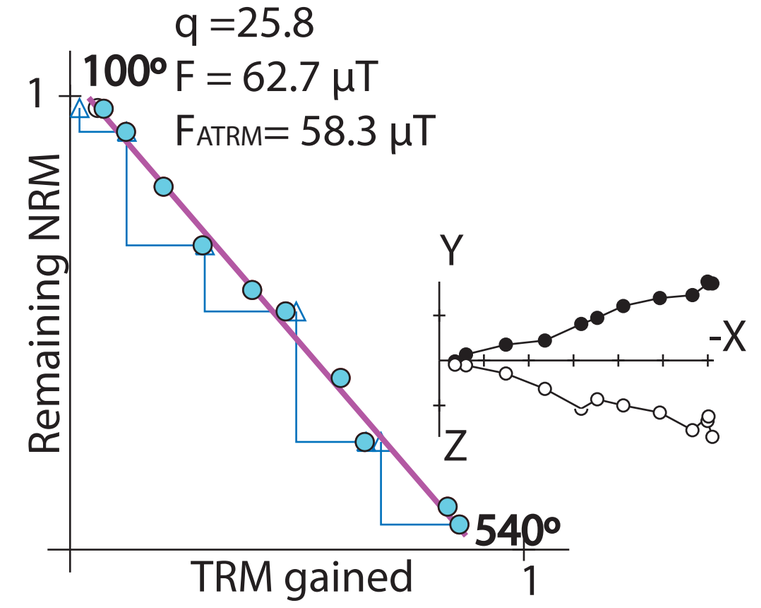
Specimen: PO-7A
NRM = 6.8•10-3 Am2/kg
q =25.8
F = 62.7 µT
FATRM= 58.3 µT
100º
540º
Remaining NRM
TRM gained
1
Y
-X
Z

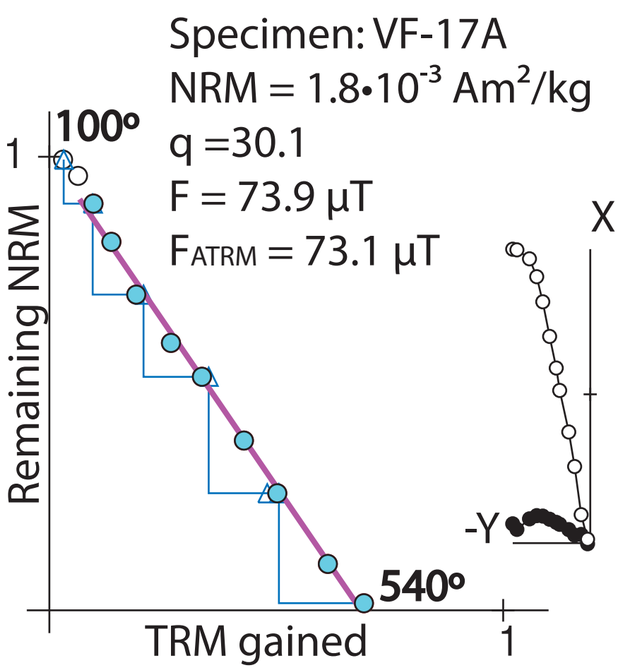
Specimen: VF-17A
NRM = 1.8•10-3 Am2/kg
q =30.1
F = 73.9 µT
FATRM = 73.1 µT
100º
540º
Remaining NRM
TRM gained
1
X
-Y

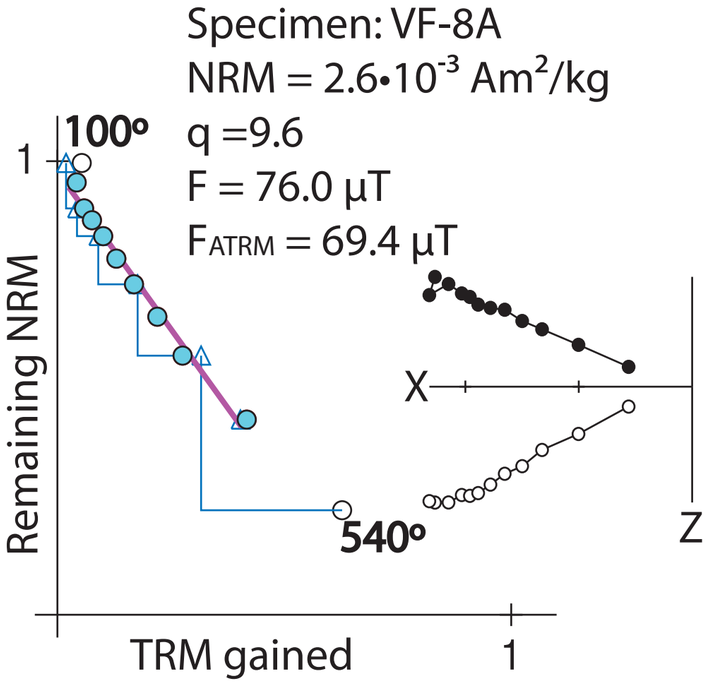
Specimen: VF-8A
NRM = 2.6•10-3 Am2/kg
q =9.6
F = 76.0 µT
FATRM = 69.4 µT
100º
540º
Remaining NRM
TRM gained
1
X
Z

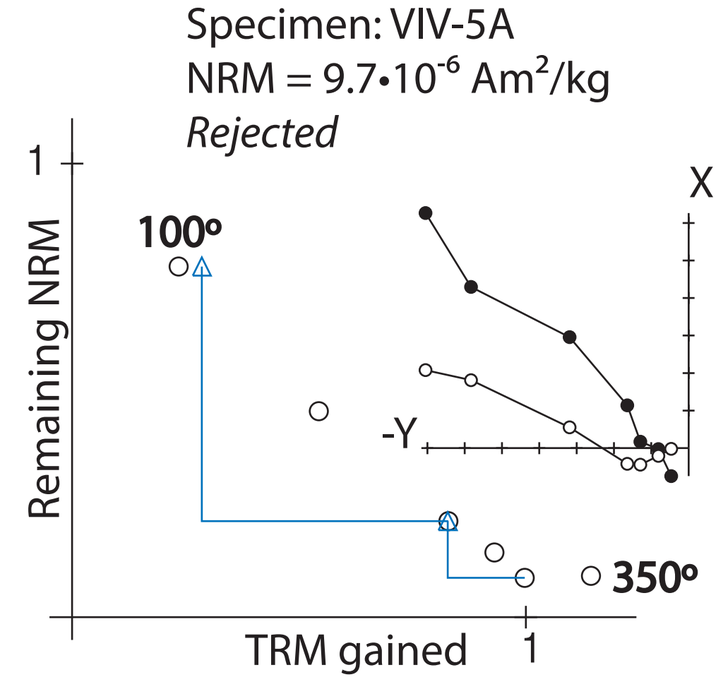
Specimen: VIV-5A
NRM = 9.7•10-6 Am2/kg
Rejected
100º
350º
Remaining NRM
TRM gained
1
X
-Y

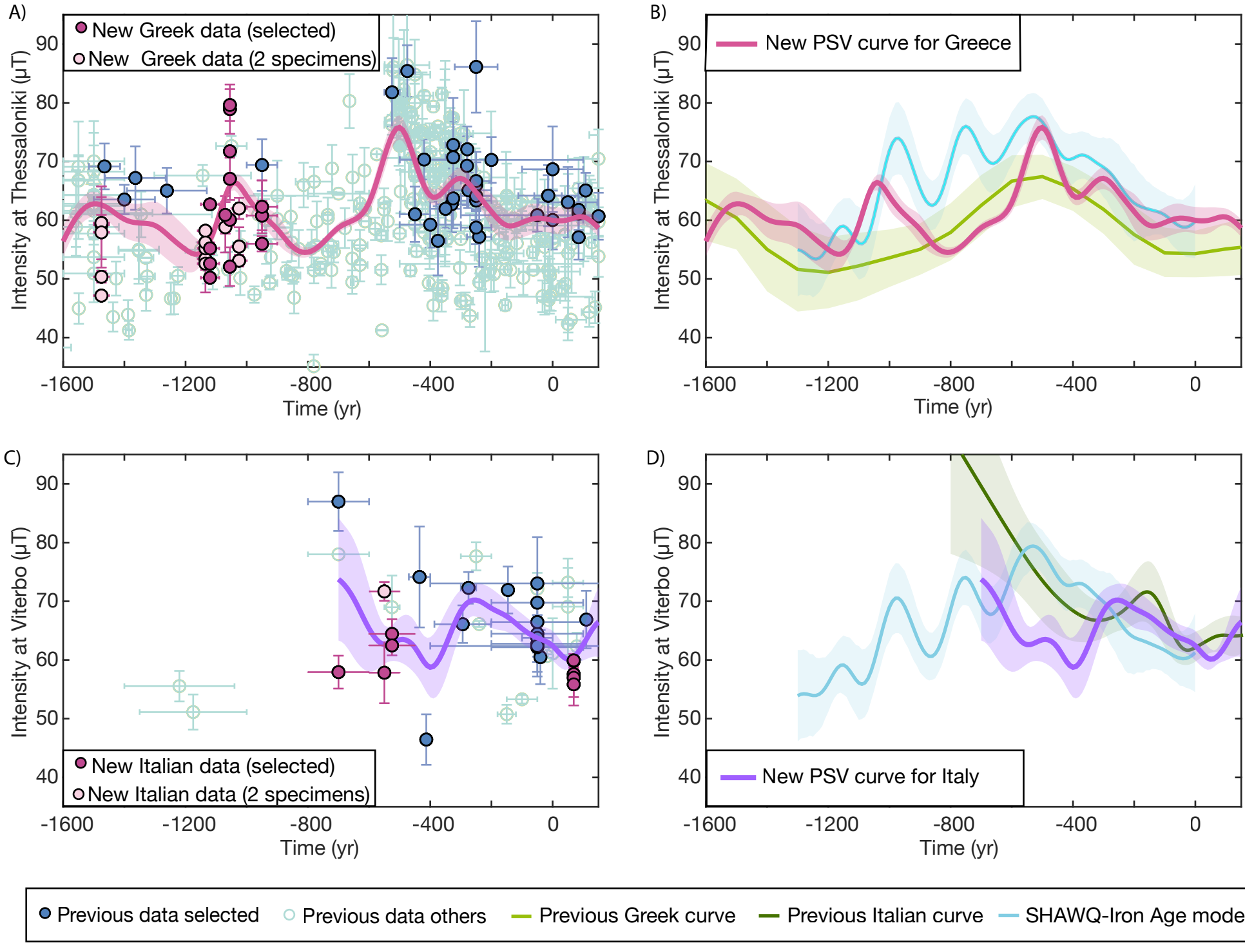
A)
New Greek data (selected)
New Greek data (2 specimens)
Intensity at Thessaloniki (μT)
Time (yr)
B)
New PSV curve for Greece
Intensity at Thessaloniki (μT)
Time (yr)
C)
New Italian data (selected)
New Italian data (2 specimens)
Intensity at Viterbo (μT)
Time (yr)
D)
New PSV curve for Italy
Intensity at Viterbo (μT)
Time (yr)
Previous data selected
Previous data others
Previous Greek curve
Previous Italian curve
SHAWQ-Iron Age model

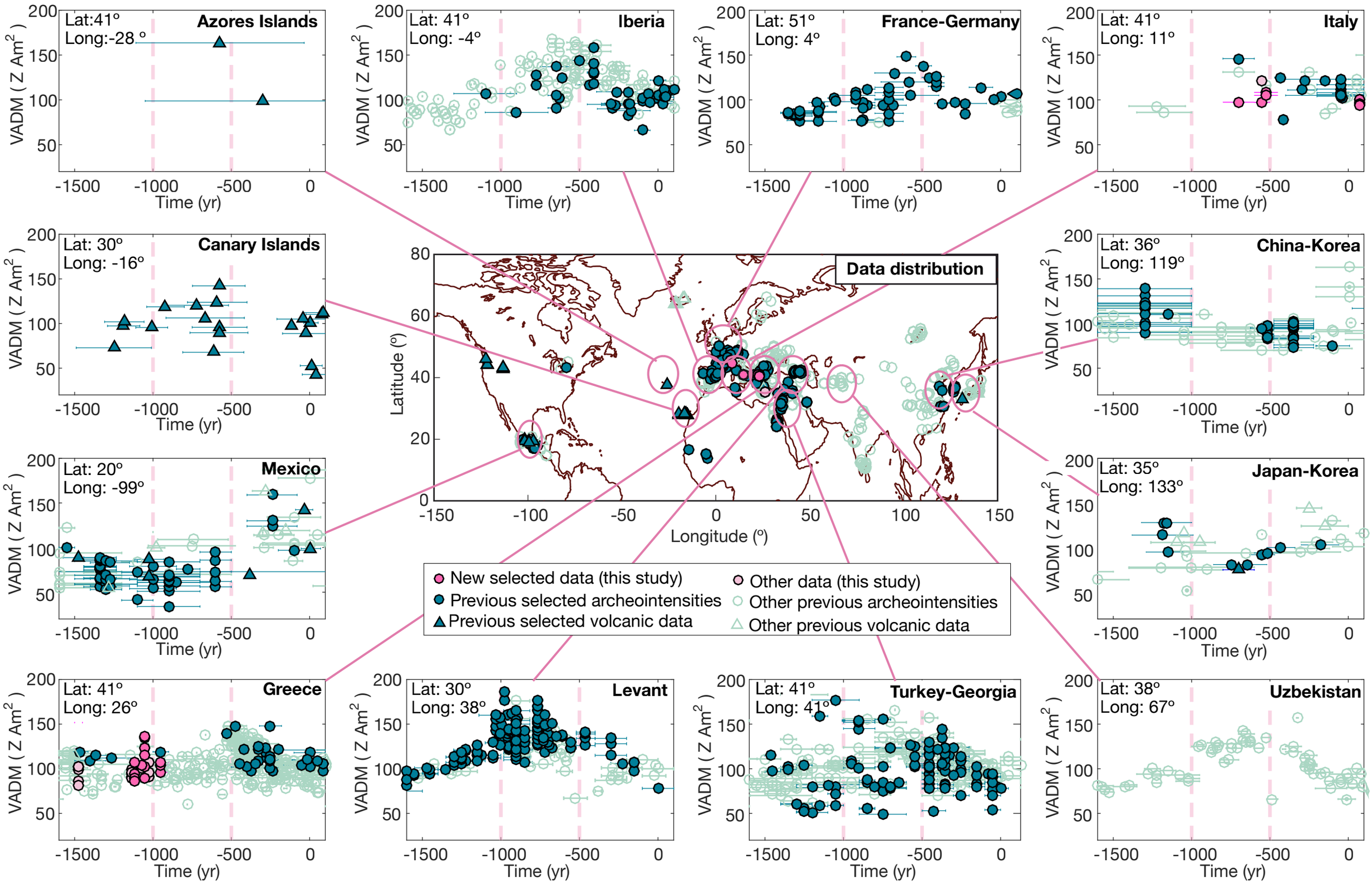
Azores Islands
Lat:41°
Long:-28 °
Iberia
Lat: 41°
Long: -4°
France-Germany
Lat: 51°
Long: 4°
Italy
Lat: 41°
Long: 11°
Canary Islands
Lat: 30°
Long: -16°
Data distribution
China-Korea
Lat: 36°
Long: 119°
Mexico
Lat: 20°
Long: -99°
Japan-Korea
Lat: 35°
Long: 133°
Greece
Lat: 41°
Long: 26°
Levant
Lat: 30°
Long: 38°
Turkey-Georgia
Lat: 41°
Long: 41°
Uzbekistan
Lat: 38°
Long: 67°
VADM (Z Am^2)
Time (yr)
Latitude (°)
Longitude (°)
New selected data (this study)
Previous selected archeointensities
Previous selected volcanic data
Other data (this study)
Other previous archeointensities
Other previous volcanic data

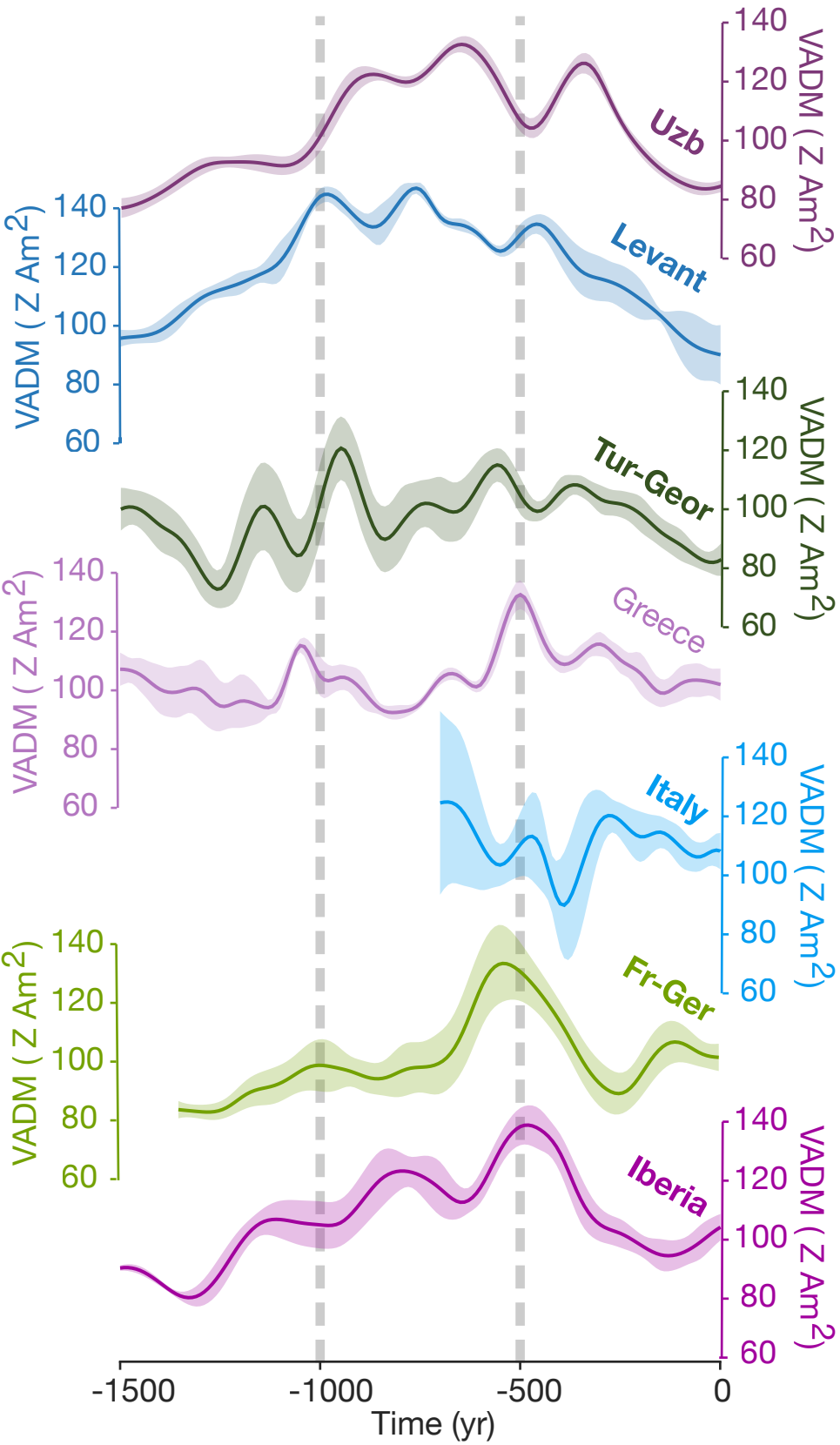
Uzb
Levant
Tur-Geor
Greece
Italy
Fr-Ger
Iberia
VADM (Z Am2)
140
120
100
80
60
-1500
-1000
-500
0
Time (yr)

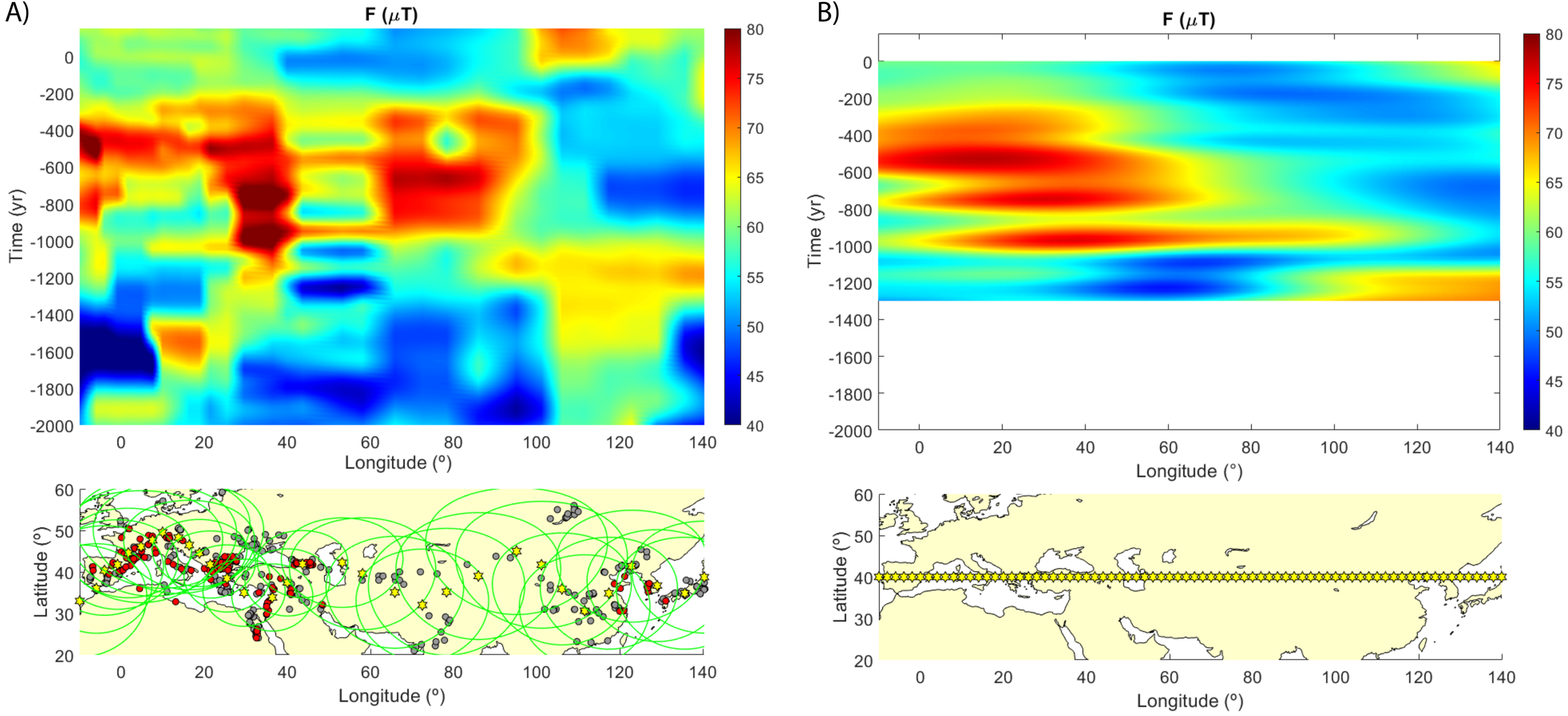
A)
F (μT)
Time (yr)
Longitude (°)
Latitude (°)
B)
F (μT)
Time (yr)
Longitude (°)
Latitude (°)

Country	Site *Lat. Long.*	Material	Lab. Code	Date (yrs BCE/CE)	N	n	F ± sd (μT)	F_{ATRM} ± sd (μT)	F_m ± sd (μT)	σ_b/F_m (%)	F_R (μT)	VADM (10^{22} Am^2)
Greece	Mochlos	Pottery	MLO 03	1500 - 1450 BCE	1	2	68.5 ± 4.0	61.1 ± 4.3	55.8 ± 6.2	11.1	59.5	10.2
	35.18ºN, 25.9ºE	Pottery	MLO 04	1500 - 1450 BCE	1	2	63.1 ± 1.4	61.1 ± 4.8	54.3 ± 6.0	11.0	57.9	9.9
		Pottery	MLO 06	1500 - 1450 BCE	1	2	51.1 ± 3.4	49.0 ± 0.5	47.2 ± 1.0	2.2	50.4	8.6
		Pottery	MLO 09	1500 - 1450 BCE	1	2	46.2 ± 5.7	49.0 ± 0.5	44.2 ± 0.5	1.0	47.2	8.1
	Toumba	Pottery	TO 15	1160 - 1110 BCE	1	2	65.9 ± 2.4	57.6 ± 2.4	53.4 ± 1.9	3.6	53.4	9.1
	40.62ºN, 22.97ºE	Pottery	TO 16	1160 - 1110 BCE	1	2	89.1 ± 0.6	66.2 ± 1.2	58.2 ± 0.2	0.4	58.2	10.0
		Pottery	TO 17	1160 - 1110 BCE	1	2	80.4 ± 1.8	62.3 ± 2.9	55.2 ± 1.1	1.9	55.2	9.5
		Pottery	TO 18	1160 - 1110 BCE	1	2	69.5 ± 0.9	60.2 ± 4.0	52.6 ± 4.9	9.4	52.6	9.0
		Pottery	TO 20	1160 - 1110 BCE	1	2	85.6 ± 2.1	64.0 ± 0.5	56.2 ± 0.6	1.7	56.2	9.6
		Pottery	TO 10	1150 - 1090 BCE	1	3	118.3 ± 4.0	70.7 ± 0.3	62.7 ± 0.4	0.7	62.7	10.7
		Pottery	TO 11	1150 - 1090 BCE	1	3	84.8 ± 8.1	63.1 ± 0.4	55.2 ± 1.0	1.9	55.2	9.5
		Pottery	TO 13	1150 - 1090 BCE	1	3	74.2 ± 5.9	65.9 ± 3.3	52.6 ± 2.3	4.3	52.6	9.0
		Pottery	TO 14	1150 - 1090 BCE	1	3	72.8 ± 6.0	53.9 ± 0.9	50.2 ± 0.8	1.6	50.2	8.6
		Pottery	TO 06	1090 - 1050 BCE	1	2	76.0 ± 3.8	65.1 ± 2.6	58.8 ± 4.3	7.4	58.8	10.1
		Pottery	TO 09	1090 - 1050 BCE	1	3	83.7 ± 5.4	67.9 ± 2.4	60.9 ± 3.2	5.3	60.9	10.4
		Pottery	TO 02	1050 - 1000 BCE	1	2	68.4 ± 0.1	66.2 ± 0.9	53.1 ± 1.0	1.8	53.1	9.1
		Pottery	TO 04	1050 - 1000 BCE	1	2	78.3 ± 9.7	68.0 ± 0.2	62.0 ± 1.8	2.8	62.0	10.6
		Pottery	TO 05	1050 - 1000 BCE	1	2	87.6 ± 3.4	65.1 ± 1.3	55.5 ± 3.3	5.9	55.5	9.5
	Assiros	Pottery	AS 01	1070 - 1040 BCE	1	3	85.7 ± 1.4	70.3 ± 2.4	60.2 ± 1.0	1.7	60.1	10.3
	40.82ºN, 23.02ºE	Pottery	AS 03	1070 - 1040 BCE	1	4	116.3 ± 8.8	86.1 ± 2.9	79.1 ± 4.2	5.2	78.9	13.5
		Pottery	AS 04	1070 - 1040 BCE	1	4	86.4 ± 6.8	76.1 ± 0.7	71.9 ± 0.7	0.9	71.7	12.3
		Pottery	AS 06	1070 - 1040 BCE	1	4	78.9 ± 7.7	61.1 ± 5.1	52.2 ± 3.3	6.3	52.1	8.9
		Pottery	AS 08	1070 - 1040 BCE	1	4	123.8 ± 12.3	74.1 ± 3.5	67.2 ± 3.6	5.4	67.1	11.5
		Pottery	AS 09	1070 - 1040 BCE	1	4	112.2 ± 2.5	83.6 ± 5.7	79.8 ± 2.7	3.4	79.6	13.6
	Kastanas	Pottery	KA 05	1000 - 900 BCE	1	3	75.4 ± 6.2	62.1 ± 0.6	56.1 ± 1.3	2.2	56.0	9.6
	40.80ºN, 22.63ºE	Pottery	KA 07	1000 - 900 BCE	1	4	90.6 ± 14.4	66.2 ± 4.7	60.9 ± 2.5	4.0	60.8	10.4
		Pottery	KA 08	1000 - 900 BCE	1	4	87.6 ± 11.0	68.0 ± 4.4	62.4 ± 4.5	7.2	62.3	10.7
Italy	C.T. Briccola	Pottery	CTBR 07	800 - 600 BCE	1	4	105.4 ± 7.5	72.9 ± 3.8	59.8 ± 2.8	4.6	57.9	9.7
	45.42ºN, 8.05ºE											
	C.T.Novella	Pottery	CTNV 02	600 - 500 BCE	1	4	77.3 ± 10.3	73.6 ± 5.1	59.7 ± 5.2	8.7	57.8	9.7
	45.42ºN, 8.05 ºE	Pottery	CTNV 04	600 - 500 BCE	1	2	77.9 ± 17.3	70.3 ± 1.5	74.0 ± 1.6	2.1	71.7	12.0
	Villa del Foro	Pottery	VF 08	600 - 450 BCE	1	4	80.3 ± 5.3	71.9 ± 3.2	65.9 ± 2.5	3.8	64.4	10.8
	44.53ºN, 8.32 ºE	Pottery	VF 17	600 - 450 BCE	1	4	73.2 ± 3.8	73.0 ± 2.7	63.9 ± 1.7	2.7	62.5	10.5
	Pompeii	Brick	PO 02	60 - 79 CE	1	3	65.2 ± 1.1	60.3 ± 1.5	58.7 ± 1.2	2.0	59.8	10.0
	40.75ºN, 14.5 ºE	Brick	PO 04	60 - 79 CE	1	3	63.2 ± 1.0	61.1 ± 2.8	56.5 ± 1.9	3.3	57.6	9.7
		Brick	PO 07	60 - 79 CE	1	4	63.4 ± 1.2	59.8 ± 1.3	58.8 ± 1.1	1.9	59.9	10.0
		Brick	PO 36	60 - 79 CE	1	4	61.7 ± 0.9	61.8 ± 3.3	55.9 ± 3.3	6.0	57.0	9.5
		Brick	PO 37	60 - 79 CE	1	4	56.7 ± 2.8	54.5 ± 2.8	54.8 ± 3.6	6.6	55.9	9.4

Site	Specimen	NRM (Am^2/kg)	T_{min}-T_{max} (°C)	n	f	g	q	MAD (°)	DANG (°)	k	β	F (μT)	F_{ATRM} (μT)	Cooling Rate factor (%)	Evol. Cool Rate (%)	$F_{ATRM+CR}$ (μT)
MLO	2A	0.0002	150-500	9	0.73	0.87	19.7	2.8	1.1	-0.40	-0.03	65.7	60.0	mean group		55.5
	3A	0.0001	250-500	7	0.60	0.83	10.2	2.2	1.6	-0.43	-0.05	72.5	56.8	9.4	2.7	51.5
	3B	0.0001	150-500	9	0.74	0.87	28.9	2.0	0.5	-0.45	-0.02	64.5	65.3	7.8	2.1	60.2
																55.8 ± 6.2
	4A	0.0001	200-500	8	0.61	0.83	12.4	3.1	1.9	-0.44	-0.04	64.4	65.8	mean fragment		58.5
	4B	0.0001	300-500	6	0.51	0.77	10.9	4.5	0.6	-0.45	-0.04	61.7	56.3	11.1	4.9	50.1
																54.3 ± 6.0
	5A	0.0002	100-420	8	0.72	0.82	17.9	2.1	0.9	-0.32	0.00	51.8	60.3	mean group		55.8
	6A	0.0002	100-500	10	0.90	0.82	26.7	2.1	0.9	-0.02	-0.03	47.7	49.5	3.2	0.6	47.9
	6B	0.0002	100-500	10	0.88	0.81	28.1	2.4	1.1	-0.15	-0.03	54.5	48.5	4.2	0.5	46.5
																47.2 ± 1.0
	7B	0.0002	250-460	6	0.67	0.78	8.8	4.5	0.6	-0.66	-0.06	104.5	72.4	mean group		67.0
	9A	0.0001	200-420	6	0.51	0.80	7.7	4.5	3.6	0.23	-0.05	40.5	47.4	mean group		43.9
	9B	0.0001	200-460	7	0.65	0.82	19.8	3.4	1.3	-0.06	-0.03	51.9	48.1	mean group		44.5
																44.2 ± 0.5
	10B	0.0001	300-500	6	0.66	0.79	11.4	2.5	0.4	-0.43	-0.05	102.9	89.6	mean group		82.9
TO	2A	0.0001	100-560	11	0.86	0.88	34.5	1.5	0.9	0.02	-0.02	68.3	67.1	21.9	0.9	52.4
	2B	0.0001	100-440	7	0.72	0.69	28.3	2.1	1.5	0.00	-0.02	68.4	65.2	17.5	3.5	53.8
																53.1 ± 1.0
	3A	0.0008	100-520	10	0.87	0.87	51.3	1.7	2.1	0.00	-0.01	79.7	82.7	11.1	0.3	73.6
	4A	0.0017	200-560	9	0.67	0.76	22.4	1.6	0.4	-0.44	-0.02	68.6	67.8	6.7	0.2	63.3
	4B	0.0037	200-560	9	0.92	0.85	28.8	1.9	0.8	0.03	-0.03	88.0	68.2	10.9	0.9	60.8
																62.0 ± 1.8
	5A	0.0030	200-560	9	0.73	0.86	27.5	2.0	0.3	-0.12	-0.02	91.0	66.4	13.0	0.9	57.8

5B	0.0026	250-560	7	0.64	0.79	16.1	2.6	0.3	-0.12	-0.03	84.2	63.8	16.7	2.5	53.2
															55.5 ± 3.3
6A	0.0010	150-560	10	0.39	0.88	42.4	1.2	0.3	-0.15	-0.02	79.8	67.7	8.7	0.3	61.8
6B	0.0008	150-560	9	0.86	0.78	43.1	2.6	0.1	-0.09	-0.02	72.2	62.5	10.9	1.4	55.7
															58.8 ± 4.3
8A	0.0055	100-560	11	0.87	0.89	94.5	2.8	0.3	-0.05	-0.01	69.3	56.3	2.5	0.0	54.9
9A	0.0009	150-560	10	0.84	0.88	56.7	1.7	0.5	-0.12	-0.01	79.0	66.1	9.4	1.4	59.9
9B	0.0011	250-560	7	0.64	0.83	14.7	3.7	1.9	-0.10	-0.04	89.6	70.6	8.7	1.2	64.5
9C	0.0006	150-560	9	0.85	0.85	36.7	4.2	0.5	-0.08	-0.02	82.6	67.0	13.0	1.9	58.3
															60.9 ± 3.2
10A	0.0052	100-560	11	0.95	0.86	59.1	1.7	0.4	-0.07	-0.01	120.7	70.4	10.6	0.7	62.9
10B	0.0054	250-560	7	0.86	0.82	31.4	2.6	0.4	-0.01	-0.02	120.5	70.9	12.3	1.8	62.2
10C	0.0045	100-560	10	0.93	0.84	63.2	2.7	1.1	-0.04	-0.01	113.6	70.9	11.2	1.6	63.0
															62.7 ± 0.4
11A	0.0011	250-560	8	0.83	0.85	54.2	2	0.3	-0.16	-0.01	94.1	62.8	10.5	0.2	56.2
11B	0.0006	250-560	7	0.82	0.83	41.4	2	0.6	-0.16	-0.02	79.9	62.9	14.0	2.9	54.1
11C	0.0014	250-560	7	0.86	0.83	30.6	1.8	0.2	-0.06	-0.02	80.4	63.6	13.3	2.9	55.1
															55.2 ± 1.0
13A	0.0002	150-560	10	0.81	0.87	28.5	1	1.2	0.08	-0.02	73.4	64.5	17.2	0.1	53.4
13B	0.0002	200-480	6	0.74	0.77	23.0	3.2	2.2	-0.03	-0.02	68.7	63.6	21.4	0.4	50.0
13C	0.0002	200-480	6	0.72	0.76	21.2	2.8	2.8	-0.14	-0.03	80.5	69.7	22.0	2.6	54.4
															52.6 ± 2.3
14A	0.0043	100-560	11	0.82	0.89	22.1	3	0.7	0.21	-0.03	69.4	54.7	6.8	2.7	51.0
14B	0.0044	100-560	10	0.78	0.87	18.8	4.2	3.8	0.19	-0.04	79.7	54.0	6.8	4.8	50.3
14C	0.0048	250-560	7	0.66	0.82	15.6	3.2	1.4	0.16	-0.03	69.2	52.9	6.6	6.3	49.4
															50.2 ± 0.8
15A	0.0016	100-560	11	0.84	0.88	37.2	1.4	0.4	-0.18	-0.02	63.5	55.2	5.7	1.1	52.0
15B	0.0018	250-560	7	0.58	0.73	12.2	2.5	0.5	-0.36	-0.03	68.3	60.0	8.7	4.2	54.8
															53.4 ± 1.9
16A	0.0010	150-560	10	0.87	0.87	54.5	1.6	1.5	-0.07	-0.01	89.7	65.0	10.2	5.0	58.4
16B	0.0013	150-560	9	0.87	0.84	43.6	2.4	1.5	-0.06	-0.02	88.5	67.3	13.7	1.5	58.1

														58.2 ± 0.2	
	17A	0.0028	150-560	560	0.93	0.85	70.8	1.4	0.7	-0.06	-0.01	78.6	59.4	8.4	2.0	54.4
	17B	0.0034	200-560	8	0.94	0.84	50.6	1.6	0.9	-0.06	-0.02	82.1	65.1	14.1	2.4	55.9
															55.2 ± 1.1	
	18A	0.0001	100-560	11	0.68	0.87	34.2	3.9	1.6	0.09	-0.02	70.4	56.2	mean fragment		49.1
	18B	0.0001	100-560	10	0.72	0.85	28.0	3.5	2.2	0.03	-0.02	68.6	64.2	12.6	6.6	56.1
															52.6 ± 4.9	
	20A	0.0004	200-560	9	0.77	0.86	27.7	2.9	2	-0.21	-0.02	87.6	63.5	10.9	0.9	56.6
	20B	0.0011	250-560	7	0.80	0.82	26.0	4.1	1.1	-0.05	-0.03	83.5	64.5	13.6	1.9	55.7
															56.2 ± 0.6	
AS	1A	0.0024	100-480	9	0.78	0.83	11.3	4.1	2.6	0.22	-0.06	84.4	67.8	9.6	6.6	61.3
	1B	0.0015	100-480	8	0.85	0.81	14.2	4.3	1.2	0.20	-0.05	87.1	72.6	18.3	3.9	59.3
	1C	0.0023	100-480	8	0.74	0.82	12.2	4.1	1.7	0.09	-0.05	85.6	70.5	14.9	4.0	60.0
															60.2 ± 1.0	
	3A	0.0002	100-480	9	0.79	0.84	18.7	1.9	4.4	0.10	-0.04	105.4	86.1	11.3	1.2	81.8
	3B	0.0001	100-430	8	0.62	0.81	24.3	4.3	8.0	-0.13	-0.02	115.3	82.7	mean fragment		74.7
	3C	0.0002	150-430	7	0.60	0.77	12.3	4.1	4.6	-0.10	-0.04	126.9	89.8	7.1	2.9	83.4
	3D	0.0002	150-430	7	0.60	0.76	15.1	3.0	5.4	-0.08	-0.03	117.5	85.7	10.6	1.4	76.6
															79.1 ± 4.2	
	4A	0.0007	300-560	7	0.87	0.76	48.2	2.5	0.4	-0.34	-0.01	89.0	76.0	5.4	4.1	71.9
	4B	0.0005	300-550	7	0.83	0.77	38.5	0.8	0.7	-0.40	-0.02	78.6	75.1	mean fragment		71.0
	4C	0.0004	300-550	7	0.81	0.78	38.3	1.5	1.0	-0.40	-0.02	83.7	76.7	mean fragment		72.6
	4D	0.0007	300-550	7	0.85	0.77	44.8	2.4	1.5	-0.38	-0.01	94.3	76.4	mean fragment		72.3
															71.9 ± 0.7	
	6A	0.0008	350-560	6	0.67	0.79	15.7	4.4	1.7	-0.96	-0.03	79.0	54.7	10.3	3.7	49.1
	6B	0.0008	350-560	6	0.65	0.79	18.8	2.9	0.8	-0.99	-0.03	71.0	59.6	15.7	5.0	50.2
	6C	0.0008	350-560	6	0.64	0.78	23.5	3.7	1.0	-0.98	-0.02	76.2	63.5	16.3	4.9	53.2
	6D	0.0009	350-560	6	0.67	0.78	26.9	2.3	1.0	-0.87	-0.02	89.4	66.6	15.3	4.5	56.4
															52.2 ± 3.3	
	8A	0.0002	150-480	8	0.66	0.85	40.6	2.1	1.8	-0.21	-0.01	113.2	74.4	11.1	4.9	66.1
	8B	0.0002	200-470	7	0.55	0.81	10.7	2.9	2.2	-0.10	-0.04	117.4	78.9	8.0	3.5	72.6

	8C	0.0002	150-470	8	0.65	0.85	13.4	4.6	0.6	-0.13	-0.04	123.4	70.9	8.7	0.7	64.7
	8D	0.0002	150-470	8	0.65	0.84	15.4	3.3	0.4	-0.19	-0.04	141.1	72.3	9.7	0.6	65.3
															67.2 ± 3.6	
	9A	0.0133	100-560	11	0.96	0.81	62.6	2.2	0.8	-0.06	-0.01	110.3	88.7	8.5	1.3	81.2
	9B	0.0201	100-550	11	0.80	0.81	65.2	4.0	0.8	-0.05	-0.01	111.5	80.4	0.4	0.4	80.0
	9C	0.0158	100-550	11	0.82	0.82	67.9	4.5	0.3	-0.01	-0.01	111.0	77.1	1.5	1.0	75.9
	9D	0.0101	100-550	11	0.91	0.81	79.6	3.0	0.8	-0.01	-0.01	115.9	88.0	6.8	0.1	82.0
															79.8 ± 2.7	
KA	5A	0.0002	150-560	10	0.58	0.87	16.7	5.0	2.4	-0.12	-0.03	77.8	61.5	10.3	1.6	55.2
	5B	0.0002	150-550	10	0.54	0.86	12.8	4.7	1.6	-0.01	-0.04	68.3	62.2	10.7	6.6	55.5
	5D	0.0002	150-550	10	0.56	0.86	11.1	3.9	1.1	0.02	-0.04	80.0	62.7	8.3	8.3	57.5
															56.1 ± 1.3	
	7A	0.0019	250-560	8	0.80	0.84	27.9	2.5	0.8	0.19	-0.02	81.1	72.5	11.4	2.5	64.2
	7B	0.0013	250-550	8	0.77	0.83	37.5	2.2	1.1	0.16	-0.02	77.7	61.3	4.3	2.8	58.7
	7C	0.0023	250-550	8	0.73	0.83	26.6	1.7	0.7	0.23	-0.02	93.9	64.9	5.8	1.8	61.1
	7D	0.0026	250-550	8	0.79	0.84	24.0	2.2	0.3	0.24	-0.03	109.5	66.2	10.2	2.8	59.5
															60.9 ± 2.5	
	8A	0.0006	150-520	9	0.77	0.86	28.3	3.3	1.0	-0.03	-0.02	88.2	72.3	12.4	1.5	63.4
	8B	0.0005	150-510	9	0.74	0.86	23.9	4.8	2.2	0.06	-0.03	72.6	64.0	10.0	1.7	57.6
	8C	0.0009	200-510	8	0.69	0.82	17.2	4.2	1.8	0.06	-0.03	99.0	71.1	4.1	0.8	68.2
	8D	0.0007	250-550	8	0.69	0.84	28.8	2.9	2.4	0.07	-0.02	90.7	64.4	6.3	0.7	60.4
															62.4 ± 4.5	

Supplementary Table 1S: Archeointensity results for the characteristic components at specimen level of the Greek archeological sites. Site, name of the site. NRM, natural remanent magnetization. T_{min}-T_{max} (°C), temperature interval used for the slope calculation. n, number of the data point within this slope calculation. f, fraction of the NRM component used. g, gap factor. q, quality factor. MAD, maximum angle of deviation. DANG, deviation angle. k, precision parameter. β, scatter statistic (Selkin and Tauxe, 2000). F, intensity without TRM anisotropy and cooling rate corrections. F_{ATRM}, intensity with TRM anisotropy correction. CR, cooling rate factor. Evol.

Cool Rate, alteration factor occurring during the cooling rate protocol. $F_{ATRM + CR}$, intensity corrected for the TRM anisotropy and cooling rate effects.

Site	Specimen	NRM (Am^2/kg)	T_{min}-T_{max} (°C)	n	f	g	q	MAD (°)	DANG (°)	k	β	F (μT)	F_{ATRM} (μT)	CR (%)	Evol. Cool Rate (%)	$F_{ATRM+CR}$ (μT)
CTBR	7A	0.0006	150-430	7	0.55	0.83	4.8	3.8	6.4	0.16	-0.10	104.7	75.8	17.4	0.9	62.6
	7B	0.0006	100-400	5	0.64	0.70	5.6	2.0	3.6	0.17	-0.08	115.3	73.2	17.8	1.5	60.2
	7C	0.0006	100-400	5	0.60	0.69	7.2	1.5	5.9	0.13	-0.06	97.2	67.5	17.0	5.3	56.0
	7D	0.0006	100-400	5	0.65	0.71	6.0	1.6	2.5	0.09	-0.08	104.5	75.1	19.4	0.8	60.5
																59.8 ± 2.8
CTNV	2A	0.0018	200-540	9	0.80	0.87	30.8	2.6	1.6	0.07	-0.02	83.7	78.6	17.5	0.5	64.8
	2B	0.0016	100-560	9	0.93	0.86	18.9	2.2	2.0	0.17	-0.04	80.1	66.8	20.9	1.2	52.9
	2C	0.0006	100-400	5	0.57	0.70	8.5	3.3	0.5	-0.09	-0.05	83.4	76.3	22.9	0.1	58.8
	2D	0.0005	250-560	6	0.73	0.77	14.6	1.9	0.2	0.10	-0.04	62.1	72.7	14.2	0.1	62.3
																59.7 ± 5.2
	3B	0.0010	250-560	7	0.72	0.81	27.6	2.8	1.6	-0.12	-0.02	74.1	72.4	21.7	1.3	56.7
	4A	0.0007	250-540	8	0.53	0.85	4.3	4.9	6.0	0.52	-0.11	65.7	69.2	-5.4	3.3	72.9
	4B	0.0024	100-560	9	0.89	0.84	15.2	3.9	3.1	0.25	-0.05	90.1	71.3	mean fragment		75.2
																74.0 ± 1.6
VF	8A	0.0026	150-500	9	0.53	0.82	9.6	3.7	3.7	0.32	-0.05	76.0	69.4	mean fragment		63.7
	8B	0.0017	150-520	7	0.75	0.82	7.0	3.7	10.0	0.39	-0.09	75.7	69.1	6.6	0.4	64.5
	8C	0.0014	150-480	6	0.61	0.79	5.7	4.4	4.6	0.36	-0.09	86.4	73.4	9.9	1.0	66.1
	8D	0.0022	150-480	6	0.57	0.79	4.7	4.7	9.1	0.39	-0.09	83.1	75.6	8.2	0.9	69.4
																65.9 ± 2.5
	17A	0.0018	200-540	9	0.87	0.87	30.1	1.4	0.8	0.10	-0.03	73.9	73.1	9.8	8.4	65.9
	17B	0.0011	150-560	8	0.89	0.85	21.0	2.3	0.8	0.12	-0.04	77.3	76.0	15.0	0.9	64.6
	17C	0.0012	150-520	7	0.79	0.83	18.3	3.3	2.0	0.08	-0.04	68.2	69.4	9.2	-0.5	63.0
	17D	0.0011	150-560	8	0.90	0.85	28.6	1.7	0.8	0.08	-0.03	73.5	73.5	15.7	1.6	62.0
																63.9 ± 1.7
PO	2A	0.0015	150-390	6	0.70	0.79	8.8	3.9	3.6	-0.34	-0.06	65.8	61.7	mean fragment		60.0
	2B	0.0013	150-480	6	0.77	0.70	20.0	2.6	1.0	-0.13	-0.03	65.9	60.5	3.5	1.1	58.4
	2C	0.0014	100-480	7	0.85	0.74	16.4	4.6	1.7	-0.08	-0.04	63.9	58.8	1.9	0.3	57.7
																58.7 ± 1.2

4B	0.0005	150-560	8	0.79	0.85	19.9	3.5	0.7	0.10	-0.03	64.3	63.3	11.5	2.7	56.0
4C	0.0007	150-480	8	0.80	0.81	16.8	2.9	0.5	-0.04	-0.04	62.9	57.9	5.2	1.8	54.9
4D	0.0005	150-560	8	0.81	0.84	58.2	2.9	2.1	-0.02	-0.01	62.3	62.0	5.4	2.7	58.6
															56.5 ± 1.9
7A	0.0068	150-540	10	0.87	0.87	25.8	4.2	1.3	-0.01	-0.03	62.7	58.3	mean fragment		57.3
7B	0.0082	100-560	9	0.96	0.85	103.7	2.1	0.7	0.00	-0.01	64.6	59.2	1.0	1.8	58.6
7C	0.0065	100-560	9	0.97	0.85	41.3	0.8	0.2	0.10	-0.02	62.1	60.9	2.3	0.5	59.5
7D	0.0083	100-560	9	0.97	0.85	84.4	2.1	0.4	0.02	-0.01	64.2	60.9	1.8	0.7	59.8
															58.8 ± 1.1
36A	0.0013	150-540	10	0.82	0.87	14.0	3.7	1.9	-0.05	-0.05	62.6	66.3	mean fragment		60.0
36B	0.0013	150-560	8	0.87	0.84	35.6	4.9	2.1	-0.03	-0.02	62.3	61.2	10.3	-0.8	54.9
36C	0.0012	150-560	8	0.87	0.84	43.6	4.1	2.1	-0.03	-0.02	61.4	58.3	10.8	-0.1	52.0
36D	0.0015	150-560	8	0.85	0.85	46.7	2.1	1.4	-0.11	-0.02	60.5	61.4	7.6	0.0	56.7
															55.9 ± 3.3
37A	0.0037	100-390	7	0.79	0.81	40.1	3.8	1.2	-0.07	-0.02	60.3	58.6	mean fragment		60.2
37B	0.0079	150-440	5	0.77	0.71	19.0	1.7	0.6	-0.04	-0.03	57.5	53.7	0.3	0.7	53.5
37C	0.0079	150-480	6	0.86	0.75	29.1	1.0	0.5	0.01	-0.02	54.5	53.1	0.6	0.9	52.8
37D	0.0076	150-480	6	0.84	0.75	28.6	1.0	0.5	0.00	-0.02	54.3	52.6	-0.3	-0.2	52.7
															54.8 ± 3.6

Supplementary Table 2S: Archeointensity results for the characteristic components at specimen level of the Italian archeological sites. Site, name of the site. NRM, natural remanent magnetization. T_{min}-T_{max} (°C), temperature interval used for the slope calculation. n, number of the data point within this slope calculation. f, fraction of the NRM component used. g, gap factor. q, quality factor. MAD, maximum angle of deviation. DANG, deviation angle. k, precision parameter. β, scatter statistic (Selkin and Tauxe, 2000). F, intensity without TRM anisotropy and cooling rate corrections. F_{ATRM}, intensity with TRM anisotropy correction. CR, cooling rate factor. Evol.

Cool Rate, alteration factor occurring during the cooling rate protocol. $F_{ATRM + CR}$, intensity corrected for the TRM anisotropy and cooling rate effects.

Supporting Information for

Geomagnetic field intensity changes in the Central Mediterranean between 1500 BCE and 150 CE: implications for the Levantine Iron Age Anomaly evolution.

M. Rivero-Montero[1], M. Gómez-Paccard[1], D. Kondopoulou[2], E. Tema[3,4], F.J. Pavón-Carrasco[1,5], E. Aidona[2], S.A. Campuzano[1], A. Molina-Cardín[1,5], M.L. Osete[1,5], A. Palencia-Ortas[1,5], F. Martín-Hernández[1,5], F. Rubat-Borel[6], M. Venturino[7]

[1]Instituto de Geociencias IGEO (CSIC-UCM), c/Doctor Severo Ochoa, 7, Edificio Entrepabellones 7 y 8, Ciudad Universitaria, 28040 Madrid, Spain.

E-mail addresses: m.rivero@csic.es; mgomezpaccard@csic.es; fjpavon@ucm.es; saioa.arquero@igeo.ucm-csic.es; amcardin@ucm.es; mlosete@ucm.es; ali@ucm.es; fatima@ucm.es.

[2]Aristotle University of Thessaloniki, Department of Geophysics, School of Geology, 54124 Thessaloniki, Greece. E-mail: despi@geo.auth.gr; aidona@geo.auth.gr.

[3]Università degli Studi di Torino, Dipartimento di Scienze della Terra, Via Valperga Caluso 35, 10125 Torino, Italy. E-mail: evdokia.tema@unito.it.

[4]Alpine Laboratory of Paleomagnetism ALP-CIMaN, Via G.U. Massa 6, 12016 Peveragno, Italy

[5]Facultad de CC. Físicas, Dpto. de Física de la Tierra y Astrofísica, Universidad Complutense de Madrid, Avd. Complutense s/n, 28040-Madrid, Spain.

[6]Soprintendenza Archeologia Belle Arti e Paesaggio per la Città Metropolitana di Torino, Piazza San Giovanni 2, 10095 Torino, Italy. E-mail: francesco.rubatborel@beniculturali.it.

[7]Soprintendenza Archeologia, Belle arti e Paesaggio per le province di Alessandria, Asti e Cuneo, Via Pavia, 15121 Alessandria, Italy. E-mail: marica.venturino@beniculturali.it

1. Archeological background and dating

The specific details of the studied archeological sites together with the geochronological constraints are given below.

A) Mochlos (MLO, Greece): 1500-1450 BCE.

The excavation at Mochlos, NE Crete (Fig. 1), is a long-standing project of the American School of Classical Studies at Athens and the INSTAP (Institute for Aegean Prehistory) Research Foundation. An extended settlement was unearthed both on the islet and on the coastal part of the modern village. The site has been extensively studied and has given ground to a serie of publications (e.g. Soles et al., 2004). The occupation of the site covers a long period spanning from the Pre-Palatial (3200-2000 BCE) to the Sub-Minoan (1000 BCE) periods. Important findings at Mochlos were the Artisan's Quarter on the mainland and a farmer's house at Chalinomouri, some 4 km east of Mochlos. In a previous research Tarling et al. (2004) presented the archeomagnetic study of two pottery kilns sampled within this Artisan's Quarter (kilns ML3 and ML4) and a third one in the farm's house yard (ML5). Apart the obtained directions, one fragment from the ML3 kiln and one from ML5 were taken for archeointensity determination, resulting in 68.2 ± 3.9 μT and 57.7 ± 5.2 μT, respectively. The 11 fragments studied here (Fig. 2A) come from several cups, jars and cooking pots produced in the ML3 and ML4 kilns that were estimated as

contemporaneous (Tarling et al., 2004). These kilns were securely dated as Late Minoan IB (1500-1450 BCE) based on different historical and archeological constraints, as well as radiocarbon analysis (see Soles et al., 2004 for details). They were last used sometime after the fall of the Santorini "Minoan" ash over this part of Crete. The Minoan eruption is a key marker for the Bronze Age chronology of the Eastern Mediterranean realm and it occurred during the mature phase of the Late Minoan IA period (1600-1500 BCE). Moreover, archeological constraints indicate that the studied kilns were no longer in operation at the time of the final destruction of the site, sometime between 1505-1430 BCE. Altogether, the archeological and radiocarbon information allows considering the final age ascribed for our studied samples as the interval 1500-1450 BCE.

B) Thessaloniki Toumba (TO, Greece): 1160-1110 BCE, 1150-1090 BCE, 1090-1050 and 1050-1000 BCE.

In Central Greek Macedonia, the usual habitations during the Early Iron Age were in the form of mounds or tells (the Greek term "Toumba" is often used as well) offering the advantage of long and continuous stratigraphic levels often well-dated and thoroughly studied (Andreou et al., 2001; Andreou, 2010). The tell of Thessaloniki Toumba, together with several others including the sites of Assiros and Kastanas also studied here, contributed to the establishment of chronological sequences which are largely used as reference for the whole Aegean, the Balkan hinterland but also the Eastern Mediterranean (Andreou, 2014 and references therein). The archeological site of Toumba, in eastern Thessaloniki, is located almost 1.5 km from the present coast of the Thermaikos bay and is one of the largest tells in Central Greek Macedonia (Fig. 1). The excavations performed in the site revealed that it was first occupied at the end of the Early Bronze Age with a

continuous use until the end of the 4th century BCE, when the mound was abandoned. The ceramics studied here belong to the deposits found in the summit of the mound where the occupation was restricted during the Late Bronze Age (Andreou and Psaraki 2007 and references therein). From this deposit we studied 19 fragments belonging to different phases (Fig. 2A). All of them are wheel made pottery from phases 4 to 2, with ages ranging from 1160 BCE (phase 4) to 1000 BCE (phase 2). Older potteries corresponding to phase 4 (1160-1110 BCE) are finer grained, with smoothed surfaces and are decorated with fine red-orange pastes and dull reddish paints. In phase 3 (1150-1090 BCE) significant changes can be observed in the technology as their pastes are less fine grained but are better fired. In phases 2 (divided in 2a: 1090-1050 BCE and 2b: 1050-1000 BCE), the common characteristic is again the drop-in quality in terms of coarseness, surface treatment and paint application, while in other aspects, such as firing, standards remained high or even improved. It seems that these changes are associated with a larger production which is in good agreement with the observation regarding the increase of wheel made pottery during the phases 2b and 2a (Andreou, 2007).

C) Assiros (AS, Greece): 1070-1040 BCE.

Assiros (AS) is a mound of average size, located about 25 km northeast of Thessaloniki city, and hosting a settlement with repeated reconstructions (Fig. 1). This settlement appears to be continuously occupied since its beginning at 2000 BCE until the Early Iron Age (around 1000 BCE) according to a robust series of radiocarbon determinations published by Wardle et al. (2014). Excavations in the site lasted 14 years by joined teams of Birmingham University and the British School at Athens. The early levels could not be properly reached and the bulk of the explored levels cover nine occupation phases

from 1400-1000 BCE that is the end of Bronze Age and the very beginning of Iron Age in Greece. The outcome of this research provides a large series of radiocarbon dates in a single, stratified site, which is unique in the Eastern Mediterranean and improves considerably our knowledge on the Greek Bronze Age. The arising chronology is compared with the neighbouring contemporaneous sites of Kastanas and Thessaloniki Toumba (Wardle et al., 2014). The studied material contains 9 fragments of hand-made sherds of local origin (see Fig. 2A) as is the 90% of the material identified in the site. The samples selected were all non-joining fragments from complete pots found shattered in the Phase 2 floors, room 2, whose construction has been dated by a combination of ^{14}C and dendrochronology at 1070-1040 BCE. Although it is theoretically possible that these vessels had been in use for some time, the balance of probability is that they were made after this age, since the structures of the preceding phase had been destroyed in an extensive fire (K. Wardle, pers. communication, 2020). The sherds, all of Iron Age fabric types, are certainly not residual material from earlier Phases.

Based on timbers, which were cut at 1070 BCE (as dated by radiocarbon and dendrochronology) the pots should have been made around that time. As the time span between their fabrication and the destruction fire which left all the pots on the floors is between 20-30 years (estimated duration of phase 2, Wardle et al., 2014, S1) the dating of the studied collection can be safely placed between 1070 and 1040 BCE.

D) Kastanas (KA, Greece): 1000-900 BCE.

The site of Kastanas is a small tell formed in an islet within the Lower Axios river during the Bronze Age. This islet is now part of the land and comprises 28 levels covering the

periods from the Late Bronze Age to the Archaic. Twelve among these levels are attributed to the Early Iron Age (Gimatzidis, 2014 and references therein). Here, we studied 16 non-decorated sherds (Fig. 2A) corresponding to the transition from the Protogeometric to the sub-protogeometric (subdivisions of the Greek Early Iron Age) that is from levels 9 and 12, dated between 1000 and 900 BCE (Hochstetter, 1984). The pottery is hand-made, mostly brown coloured, and includes several forms: handles, glazed sherds from table pots, bowls and a few possibly cooking pots.

E) Viverone (VIV, Italy): 1450-1400 BCE.

The site of Vi1-Emissario (Viverone) is part of the Prehistoric pile dwellings around the Alps (*palafitte* in Italian) that comprise a series of 111 archeological sites identified within the European Alps. These settlements, dispersed throughout Switzerland, Austria, France, Germany, Slovenia and Italy, are a UNESCO World Heritage Site since 2011. The archeological site Vi1-Emissario is about 3600 m^2 wide and lies on the bottom of Lake Viverone between 2 and 3 m deep (Fig. 1). Lake Viverone is located in a large Alpine morainic amphitheatre in Piedmont, in northwestern Italy. After the first investigations carried out at the 70s and 80s, the site was systematically studied between 2011 and 2016 by the Soprintendenza Archeologia Belle Arti e Paesaggio per la Città Metropolitana di Torino and the Universities of Basel and Bradford. The rich archeological collection composed of over 200 bronze artefacts and at least 5000 ceramic sherds, of which a thousand are carefully studied, can be culturally placed in the Italian Middle Bronze Age 2, contemporary with the end of the northern Alpine subphases BzC1, thanks to numerous comparisons with other sites and cultural areas. Moreover, 145 oak piles were dated by dendrochronology. The Viverone dendrochronological sequences

could not be correlated with the Nord Alpine sequences (a common problem in several other sites in northern Italy, as for example the area around Garda Lake, Billamboz and Martinelli, 2015) and therefore local sequences were produced through wiggle-matching based on three independent radiocarbon analysis (3271 ± 22 (Hd-30412); 3135 ± 24 (Hd-30411); 3219 ± 33 (Hd-30413) uncalibrated yrs BP, see Rubat Borel et al., 2016 for details). The obtained results date the oak piles between 1438 and 1401 cal BCE. The possibility of crossing the absolute dating given by radiocarbon and dendrochronology with the relative chronology of the archeological finds makes Viverone a key site for the chronological reconstruction of the European Bronze Age (Rubat Borel, 2010; Rubat Borel et al., 2016). Some more ancient finds, belonging to Neolithic (dating from the first half of the 5th millennium BCE), and to the Late Bronze Age (second half of the 11th century BCE), were also found in the site. In this study we have selected and studied 17 pottery sherds (Fig. 2B) that clearly belong to the late 15th century BCE occupation phase and can be safely dated at 1450-1400 BCE.

F) Castelletto Ticino: Briccola (CTBR, Italy): 800-600 BCE and Ticino Novella (CTNV, Italy): 600-500 BCE.

Castelletto Ticino is situated at Novara Province, in Piedmont (Fig.1), between Lake Maggiore, Ticino river and Novara city. It is an important archeological site dated as between the end of the 9th century BCE and the beginning of the 5th century BCE (until 480 BCE). The site hosted a large settlement of the Golasecca culture. The Golasecca culture was an Early Iron Age culture in northern Italy, speaking a Celtic language, and for several centuries it acted as a link between the Etruscan-Italic world and the cultures of central-western Europe. Thanks to the rich archeological findings found in the area, a

very fine archeological chronology with 50-70 years wide phases, was developed (De Marinis and Gambari, 2005). Such chronology is mainly based on ceramic and metal funerary objects from incineration tombs (Spagnolo-Garzoli and Gambari, 2004). For this study, 22 pottery sherds (Fig. 2B) from two separate contexts of the settlement were collected: Briccola and Ticino Novelli. Both contexts are located in the northern area of the Castelletto Ticino archeological site, on a terrace of the Ticino river in glacio-lacustrine deposits of sand and silt. The pottery collected from Briccola is dated between 800 and 600 BCE, while the pottery fragments from Ticino Novelli are slightly younger, dated between 600 and 500 BCE, based on the stratigraphy and diagnostic archeological artefacts found at the site (Spagnolo-Garzoli and Gambari, 2004).

G) Villa del Foro (VF, Italy): 600-450 BCE.

The archeological site of Villa del Foro (VF) is situated near the city of Alessandria, in Piedmont, northern Italy (Fig. 1). Several archeological excavation campaigns carried out since the early 80's brought to light an important Iron Age settlement (Venturino Gambari, 1986). The archeological findings, which are very rich and include several furnaces, small combustion structures, pottery sherds and a large number of characteristic ring-shaped ceramic artefacts, give evidence of the presence of an important ancient workshop used for clay elaboration and pottery production (Venturino Gambari, 1993). In the northern part of the archeological site and mostly in the proximity of the combustion structures, clear traces of fire are found together with a large number of pottery fragments, both coarse and fine grained. Based on the ceramic findings made of local clay and mainly used for domestic use, together with the significant presence of black and glossy bucchero wares, the occupation of the site is dated at the 6th up to the

first half of the 5th century BCE (Venturino Gambari et al., 2010). The most recent excavation at Villa del Foro was carried out in 2007-2008 in the occasion of public works for the installation of gas pipes. The new findings, that include clay pits, water wells as well as more combustion structures and ceramics offer further evidence for the use of the site as pottery production workshop while the findings of slags do not exclude also a metallurgic activity. For this study, a total of 18 pottery fragments (US 2239) were collected and analysed, all dated at 600-450 BCE (Fig. 2B).

H) Pompeii (PO, Italy): 60-79 CE.

Pompeii is one of the most well-known archeological sites in Italy, situated near the city of Naples (Fig.1). The first excavations of the ancient city began in the 18th century and since then numerous archeological campaigns brought to light a large part of the Roman city that was completely buried under meters of ashes and pyroclastic deposits produced during the violent 79 CE eruption of Mount Vesuvius. This famous eruption completely covered and destroyed the ancient city of Pompeii but at the same time it preserved it, offering nowadays one of the most significant remains of Roman civilization, and a unique example of exceptional ancient architecture, city organization, wall paintings and mosaics. In this study, pieces of bricks and tiles from the ruins of the ancient city were analyzed. The samples were initially collected and studied to estimate the deposition temperature of the pyroclastic products through the investigation of the secondary thermoremanent magnetization component acquired by the tiles/bricks while they were embedded into pyroclastic deposits (Zanella et al., 2007). Here, we have selected and analyzed 6 samples (Fig. 2B) that were not importantly influenced by partial re-heating and thus they were characterized by a clear single component of magnetization acquired

during their production. The exact age of the bricks and tiles manufacturing cannot be known but it could be reasonably estimated at few decades before the 79 CE eruption. Actually, Pompeii was importantly damaged due to a strong earthquake occurred on 62 CE and clear evidence of the city rebuilding between 62 CE and the eruption in 79 CE identified in the ruins could further sustain a reliable dating of the studied material around 60-79 CE

2. Methodology:

A) Paleosecular Variation curves

We calculated the paleosecular variation (PSV) intensity curves based on penalized cubic b-splines, with knot points every 50 years (Thébault and Gallet, 2010) and considering both dating and experimental uncertainties by means of a bootstrap approach. For each location, we first calculated an initial curve to check and reject possible outliers and then, the final PSV was obtained providing a mean value of the 5000 curves of intensity calculated, and the corresponding standard deviations over time. Moreover, and according to our previous results (Campuzano et al., 2019), we decided to apply a weight 10 times higher to the selected data than to the other less robust ones. These different weights are considered for the computation of the final PSV curves obtained

B) Hovmöller diagrams

The Fig. 8a in the main text of the article shows the Hovmöller diagram (Hovmöller 1949) obtained using the methodology explained in Molina-Cardin et al. (2018) and based on

the construction of PSV curves. The PSV curves (Fig. 2S) have been calculated according to the methodology explained previously in this work, from 2000 BC to 150 AD. In order to avoid possible border effects, we generate the curves using some additional data over the limits, from 2200 BC to 2000 BC and from 150 AD to 350 AD. PSV curves were calculated in the yellow stars showed on the map of fig. 8a. Then, they were relocated to a common latitude of 40º. The radius of the circle around which we computed the PSV curves (green circles in fig. 8a) determines the data with which the PSV curve was generated. It has been chosen according to the number of data around the centre. From a fixed radius of 900 km, we have calculated the number of data around the centre: the lower number of data was, the larger final radius was chosen. If the number of data was higher than 300, then the chosen radius was 900 km. If the number of data was from 300 to 200 then the chosen radius was 1200 km. In the case of number of data from 200 to 25, the radius was 1500 km and finally, for cases where the number of data was lower than 25, the radius was 1700 km. This selection is especially important in regions where the number of data is scarce, such as Central Asia.

In fig. 8b, also shown in the main manuscript, we represented the Hovmöller diagram computed from synthetic PSV curves calculated using the SHAWQ-Iron Age model (Osete et al., 2020) centred in 40º of latitude. Notice that the interval of time spanned by the model is shorter than the previous Hovmöllers, from 1300 BC to 0 AD.

Finally, the Hovmöller diagram shown in Fig. 1Sa (see below) has been directly calculated using the global dataset. For this purpose, the archeomagnetic and volcanic database GEOMAGIA50v3.3 has been updated with the most recently published data. For considering the temporal and intensity errors we have followed a Monte Carlo method

in which we have added a random error to each data considering a Gaussian distribution for the intensity (with its standard deviation corresponding to the data uncertainty) and a uniform distribution for the age, obtaining a perturbed database. This process has been repeated 10000 times. With each perturbed database, we have calculated a Hovmöller diagram as follows. The selected area (from 20°N to 60°N in latitude, from 30°W to 150°E in longitude, from 2000 BCE to 500 CE in time) has been divided in overlapping rectangular bins spanning 100 years, 20° of longitude and the whole selected range in latitude. Adjacent bin centers are spaced 5° in longitude and 20 years in time. For each bin, all the data falling within its limits has been relocated to its centre and then reduced to a weighted mean value, using a weight 10 times higher for the selected data than for the other (classified as described in section 6.1). Fig. 1Sa represents the average of all the Hovmöllers obtained following this procedure. Fig. 1Sb shows the total weight in each bin averaged over the 10000 repetitions, which provides an idea of the reliability of the mean value showed in Fig. 1Sa.

Supplementary figures

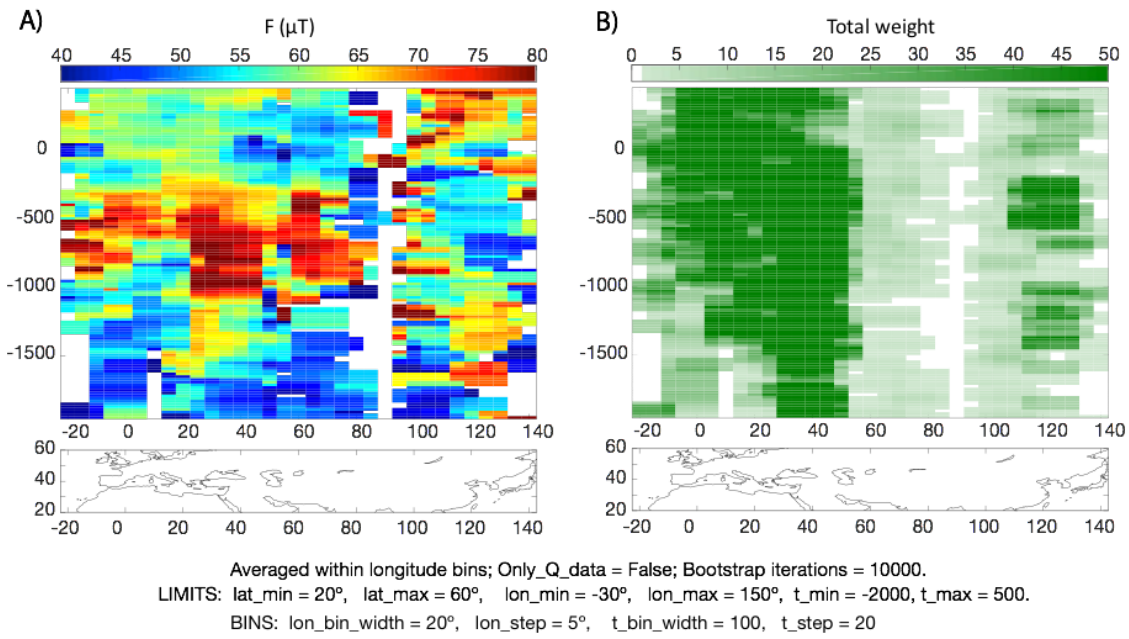

Figure 1S. Hovmöller diagrams. A) Hovmöller calculated from the archeomagnetic and volcanic database GEOMAGIA50v3.3 updated with the recently published data. B) Total weight in each bin also averaged over the 10000 repetitions. Scale is saturated at 50, which correspond to 5 selected data or 50 non-selected data (or any combination). The lighter the cell is, the less accurate the values in A are.

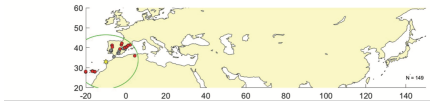
N = 149

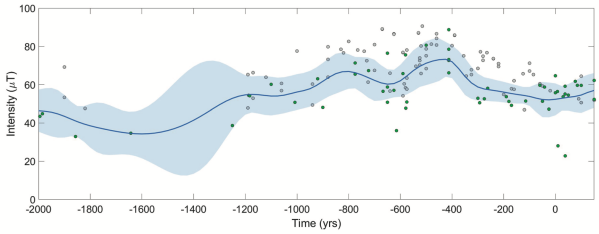
Intensity (μT)
Time (yrs)

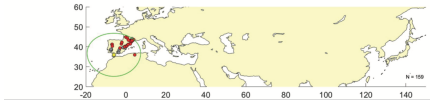
N = 159

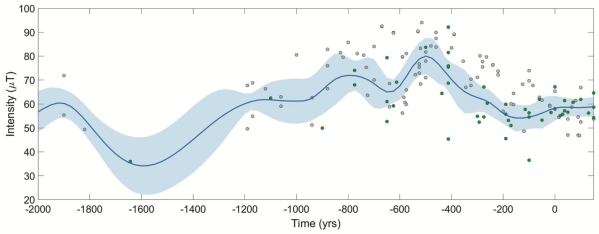
Intensity (μT)
Time (yrs)

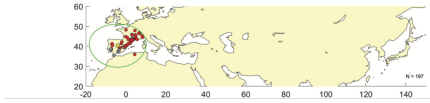
N = 197

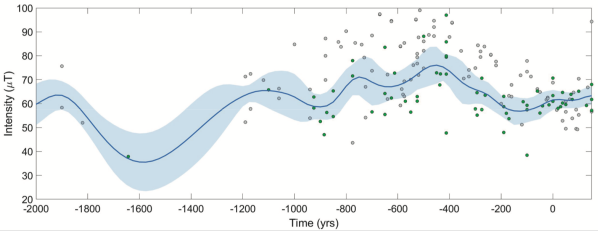
Intensity (μT)
Time (yrs)

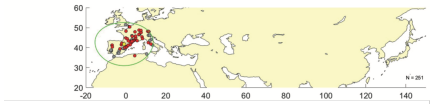
N = 251

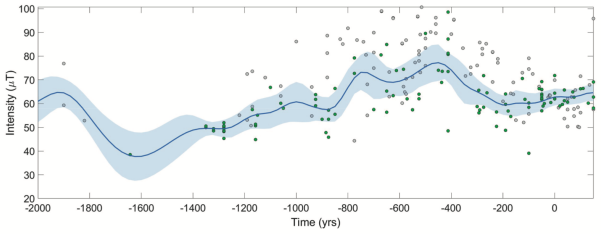
Intensity (μT)
Time (yrs)


N = 275

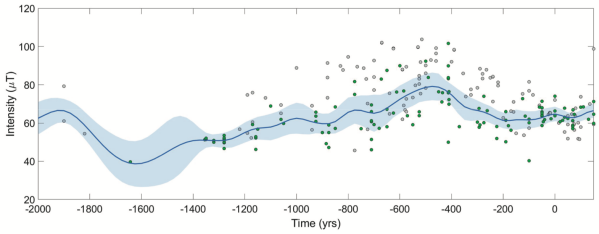
Intensity (μT)
Time (yrs)


N = 308

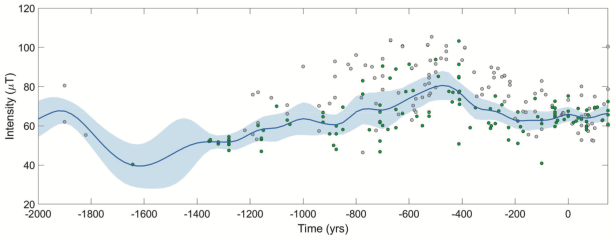
Intensity (μT)
Time (yrs)


N = 322

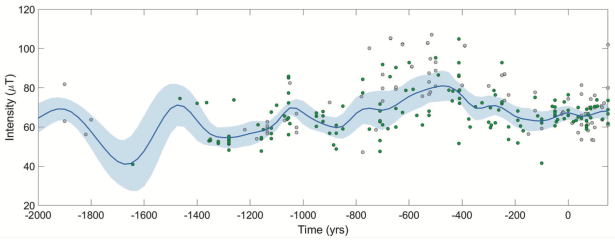
Intensity (μT)
Time (yrs)


N = 340

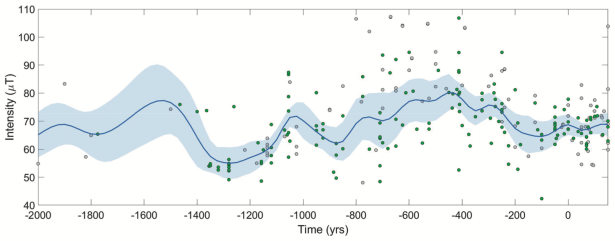
Intensity (μT)
Time (yrs)


N = 443

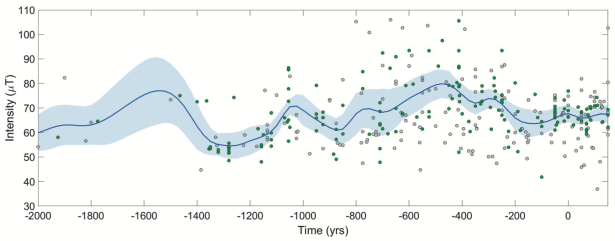
Intensity (μT)
Time (yrs)


N = 365

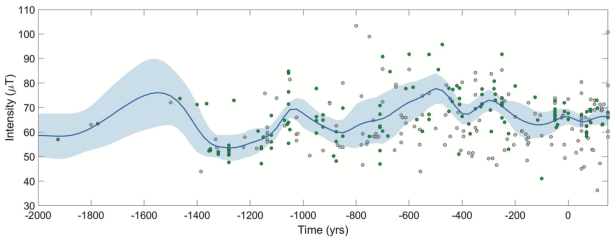
Intensity (μT)
Time (yrs)


N = 293

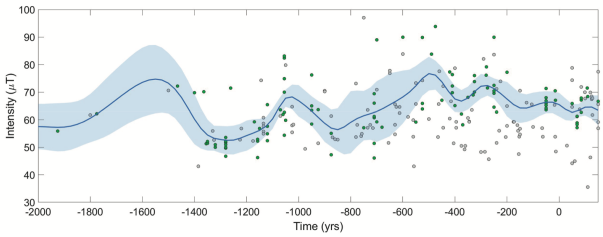
Intensity (μT)
Time (yrs)

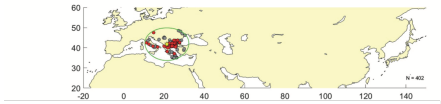
N = 402

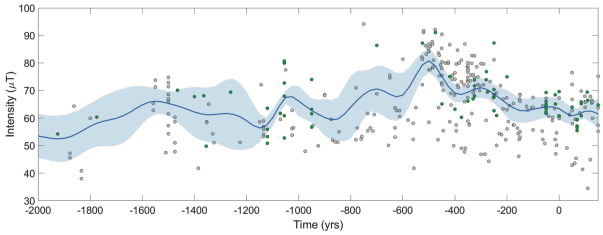
Intensity (μT)
Time (yrs)

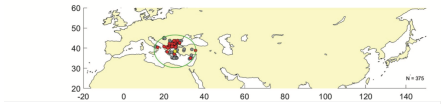
N = 375

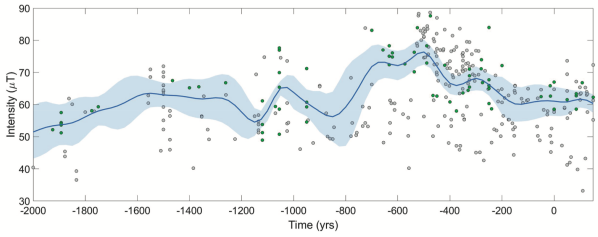
Intensity (μT)
Time (yrs)

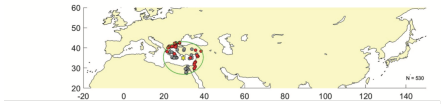
N = 530

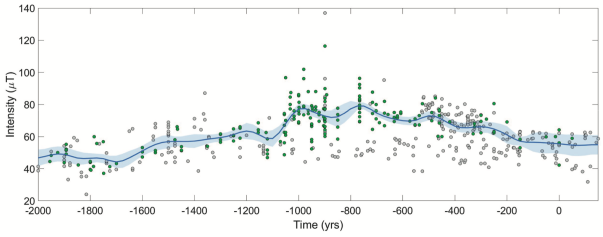
Intensity (μT)
Time (yrs)

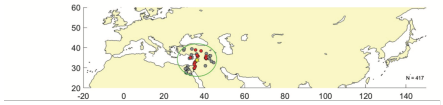
N = 417

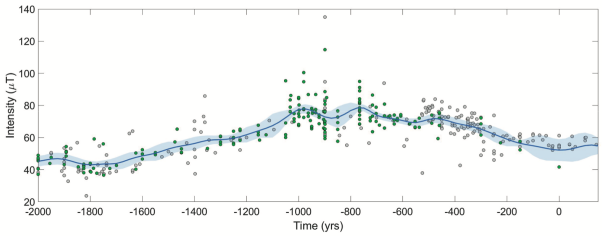
Intensity (μT)
Time (yrs)

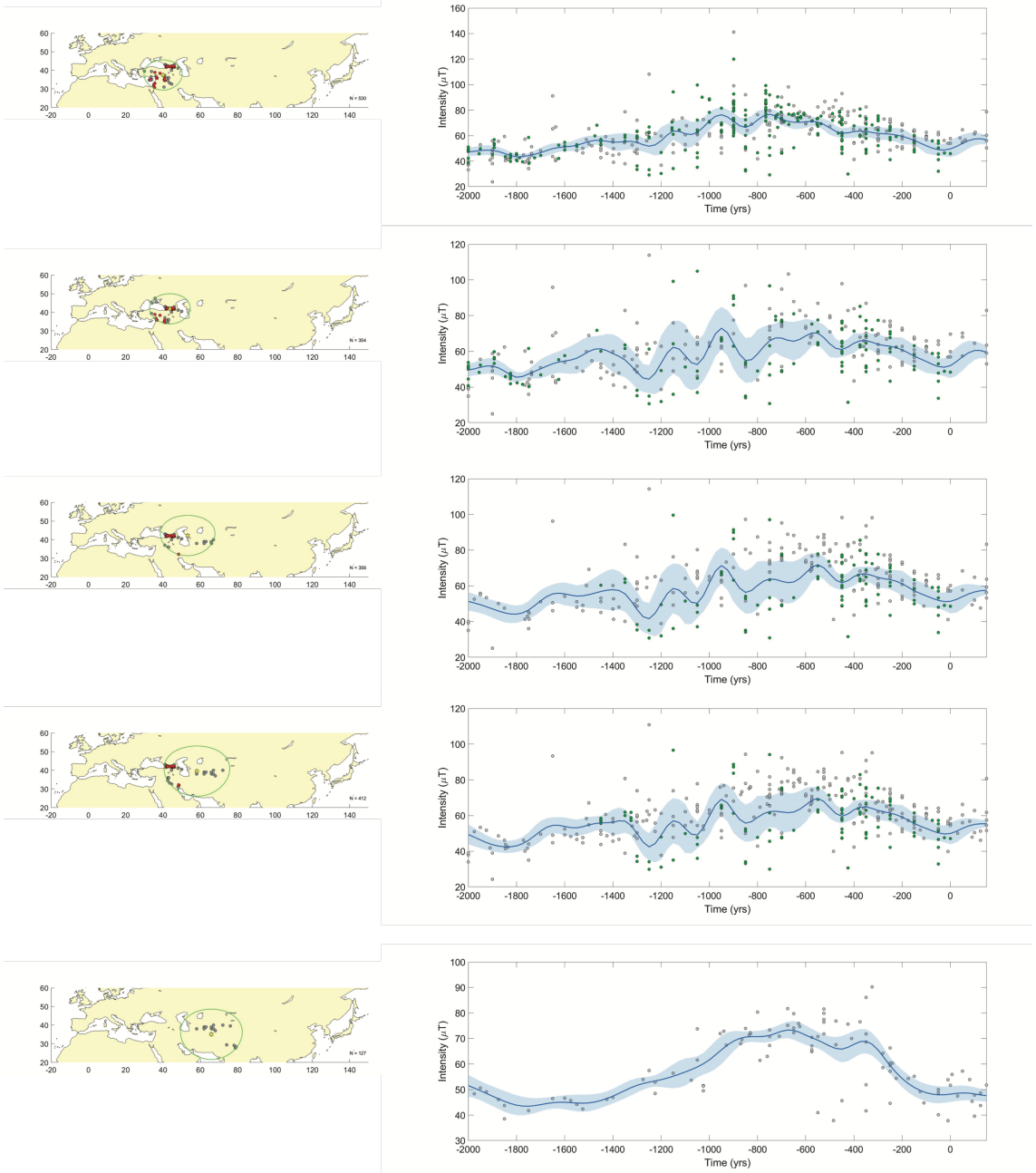
N = 530
N = 354
N = 356
N = 412
N = 127
Intensity (μT)
Time (yrs)

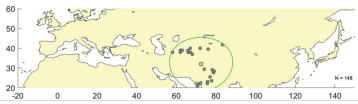
N = 148

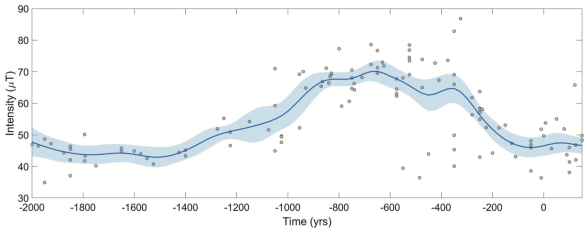
Intensity (μT)
Time (yrs)

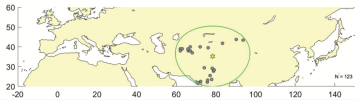
N = 123

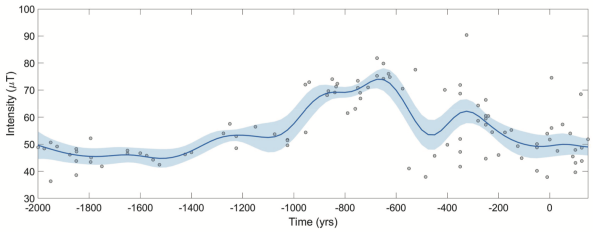
Intensity (μT)
Time (yrs)

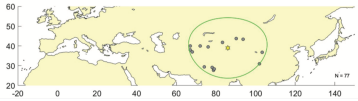
N = 77

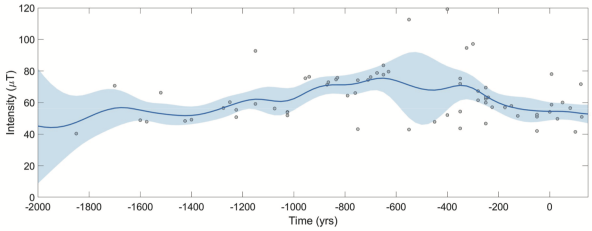
Intensity (μT)
Time (yrs)

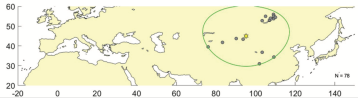
N = 78

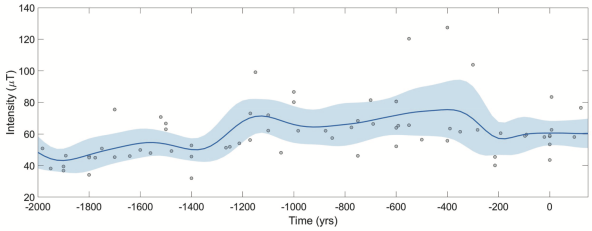
Intensity (μT)
Time (yrs)

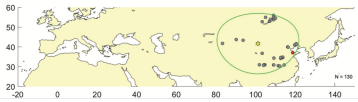
N = 130

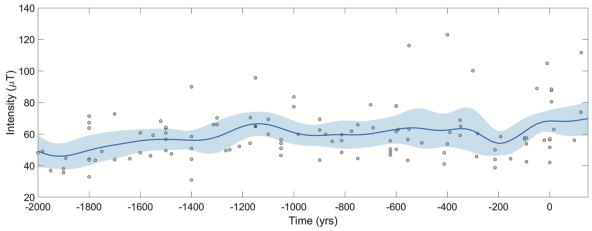
Intensity (μT)
Time (yrs)


N = 117

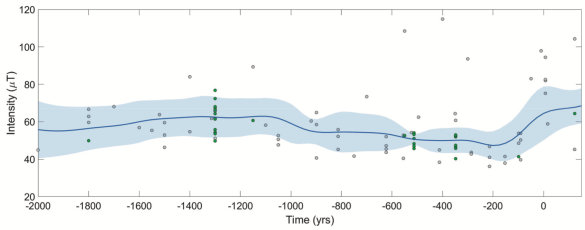
Intensity (μT)
Time (yrs)


N = 126

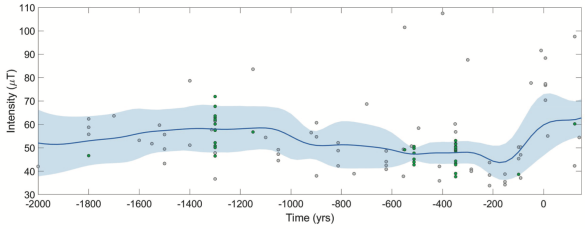
Intensity (μT)
Time (yrs)


N = 149

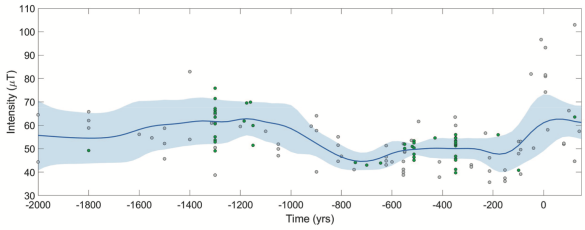
Intensity (μT)
Time (yrs)

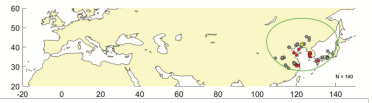
N = 140

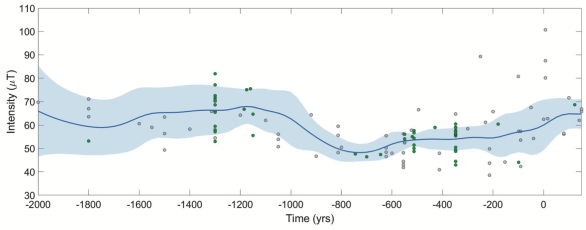
Intensity (μT)
Time (yrs)


N = 149

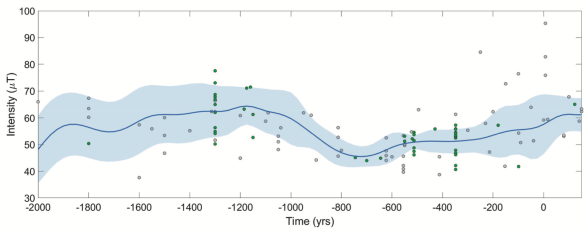
Intensity (μT)
Time (yrs)

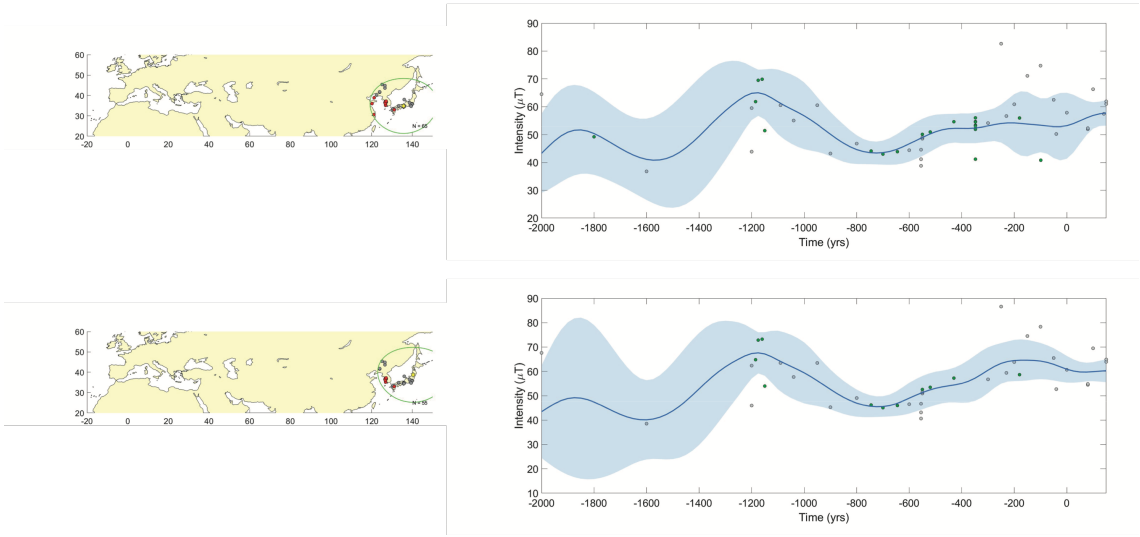

Figure 2S. PSV curves calculated according to the methodology explained in this work for the Hovmöller diagram shown in figure 8.

References

Andreou, S., Fotiadis, M., Kotsakis, K., 2001. The Neolithic and Bronze Age of Northern Greece, in T. Cullen (edit), Aegean Prehistory: A review, AJA Suppl.1, Boston, 259-328.

Andreou, S., 2007. Stratified wheel made pottery deposits and absolute chronology of the LBA to the EIA transition at Thessaloniki Toumba. In: S. Deger-Jakotzy and A. Bahle (Eds) LH III C Chronology and Synchronisms III. LH III C Late and the transition to the Early Iron Age. International workshop held at the Austrian Academy of Sciences, Vienna, 23-27 Feb., 2007, 183-202.

Andreou, S., Psaraki, K., 2007. Tradition and Innovation in the Bronze Age Pottery of the Thessaloniki Toumba. In: Stefanovich – Todorova – Ivanov (Eds) The

Struma/Strymon River Valley in Prehistory. Proceeding of the International Symposium ‘Strymon Praehistoricus, 27 Sept - 1 Oct, 2004, Sofia.

Andreou, S., 2010. Northern Aegean, in E. Cline (Editor) Oxford Handbook of Bronze Age Aegean, New York/ Oxford, 643-659.

Andreou, S., 2014. One hundred years of research in the Bronze Age of Macedonia.What changed? In E. Stefani, N. Merousis, A. Dimoula (eds) A century of Research in Prehistoric Macedonia, International Conference Proceedings, Archaeological Museum of Thessaloniki, 22-24 November 2012,141-151(in greek with English abstract).

Billamboz, A., Martinelli, N., 2015. Dendrochronology and Bronze Age pile-dwellings on both sides of the Alps. In: Menotti, F. (Eds.), The End of the Lake-dwellings on the Circum-Alpine Region, Oxford, 68-84.

Campuzano, S.A., Gómez-Paccard, M., Pavón-Carrasco, F.J., Osete, M.L., 2019. Emergence and evolution of the South Atlantic Anomaly revealed by the new paleomagnetic reconstruction SHWQ2k. Earth Planet. Sci. Lett., 512, 17-26.

De Marinis, R.C., Gambari, F.M., 2005. La cultura di Golasecca dal X agli inizi del VII secolo a.C.: cronologia relativa e correlazioni con altre aree culturali. In: Bartoloni, G., Delpino, F. (Eds.), Oriente e occidente: metodi e discipline a confronto. Riflessioni sulla cronologia dell’età del Ferro italiana, Pisa-Roma, 197-225.

Gimatzidis, S. 2014. Does time stand still in the Aegean? Early Iron Age chronology at Kastanas revisited, in E. Stefani, N. Merousis, A. Dimoula (eds) A century of Research in Prehistoric Macedonia, International Conference Proceedings, Archaeological Museum of Thessaloniki, 22-24 November 2012, 303- 312.

Hochstetter, A. 1984. Kastanas. Ausgrabungen in einem Siedlungshugel der Bronze und Eisenzeit Makedoniens 1975-1979. Die handgemachte Keramik, Prahistorische Archaeologie in Sudosteuropa 3, Berlin.

Hovmöller, E., 1949. The trough-and-ridge diagram. Tellus 1 (2), 62–66. https://doi.org/10.3402/tellusa.v1i2.8498.

Molina-Cardín, A., Campuzano, S.A., Osete, M.L., Rivero-Montero, M., Pavón-Carrasco, F.J., Palencia-Ortas, A., Martín-Hernández, F., Gómez-Paccard, M., Chauvin, A., Guerrero-Suárez, S., Pérez-Fuentes, J.C., McIntosh, G., Catanzariti, G., Sastre-Blanco, J.C., Larrazabal, J., Fernández-Martínez, V.M., Álvarez-Sanchís, J.R., Rodríguez-Hernández, J., Martín-Viso, I., García I Rubert, D., 2018. Updated Iberian archeomagnetic catalogue: new full vector paleosecular variation curve for the last three millennia. Geochem. Geophys. Geosyst., 19, 3637-3656. https://doi.org/10.1029/2018GC007781.

Osete, M.L., Molina-Cardín, A., Campuzano, S.A., Aguilella-Arzo, G., Barrachina-Ibañez, A., Fallomir-Granell, F., Olver Foix, A., Gómez-Paccard, M., Martín-Hernández, F., Palencia-Ortas, A., Pavón-Carrasco, F.J., Rivero-Montero, M. Two archaeomagnetic intensity maxima and rapid directional variation rates during the Early Iron Age observed at Iberian coordinates. Implications on the evolution of the Levantine Iron Age Anomaly. Earth Planet. Sci. Lett., 533, 116047.

Rubat Borel, F., 2010. La ceramica della Media età del Bronzo dell'abitato perilacustre di Viverone. Quaderni della Soprintendenza Archeologica del Piemonte 25, 31-70.

Rubat Borel, F., Menotti, F., Martinelli, N., Köninger, J., 2016. Viverone, sito palafitticolo. Datazioni dendrocronologiche, Quaderni della Soprintendenza Archeologica del Piemonte 31, 226-229.

Soles, J.S., Davaras, C., Bending, J., Carter, T., Kondopoulou, D., Mylona, D., Ntinou, M., Nicgorski, A.M., Reese, D.S., Sarpaki, A., Schoch W.H., Soles, M.E., Spatharas, V., Stos-Gale, Z.A., Tarling, D.H., Witmore, C., 2004. Mochlos IC. INSTAP Prehistory Monographs 9, Philadelphia.

Spagnolo-Garzoli, G., Gambari, F.M., Tra terra e acque. Carta archeologica della provincia di Novara, Novara, 2004.

Tarling, D., Kondopoulou, D., Spatharas, V., 2004. An archaeomagnetic Study of the LM IB Kilns, in J. Soles and C. Davaras (eds) MochlosIC, PeriodIII. Neopalatial Settlement on the Coast:The Artisans' Quarter and the Farmhouse at Chalinomouri, INSTAP Academic Press, Philadelphia, Pennsylvania.

Thébault, E., Gallet, Y., 2010. A bootstrap algorithm for deriving the archeomagnetic field intensity variation curve in the Middle East over the past 4 millennia BC. Geophys. Res. Lett, 37, 22.

Venturino Gambari, M., 1986. Alessandria, frazione Villa del Foro. Scavi dell'abitato della prima età del Ferro. Quaderni della Soprintendenza Archeologica del Piemonte, 7, 45–47.

Venturino Gambari, M., 1993. Alessandria, frazione Villa del Foro. Scavi nell'area dell'abitato protostorico. Quaderni della Soprintendenza Archeologica del Piemonte, 11, 204–205.

Venturino Gambari, M., Gatti S., Giaretti M., 2010. Alessandria, frazione Villa del Foro: indagini archeologiche nell'era del sito della media età del Ferro. Quaderni della Soprintendenza Archeologica del Piemonte, 25, 130–133.

Wardle, K., Highman, T., Kromer, B., 2014. Dating the End of the Greek Bronze Age: A robust Radiocarbon-Based Chronology from Assiros Toumba. PLOS One, 9 (9), e106672.

Zanella, E., Gurioli, L., Pareschi, M.T., Lanza, R., 2007. Influences of urban fabric on pyroclastic density currents at Pompeii (Italy): 2. Temperature of the deposits and hazard implications. Journal of Geophysical Research: Solid Earth, 112 (5), B05214.